Pure Appl. Geophys. 169 (2012), 101–122

DOI 10.1007/s00024-011-0321-3

Pure and Applied Geophysics

S-Wave Velocities of the Lithosphere–Asthenosphere System in the Caribbean Region

O'Leary F. González,[1,2] José Leonardo Alvarez,[1,2] Bladimir Moreno,[1,2] and Giuliano F. Panza[2,3]

Abstract—An overview of the S-wave velocity (V_s) structural model of the Caribbean with a resolution of 2° × 2° is presented. New tomographic maps of Rayleigh wave group velocity dispersion at periods ranging from 10 to 40 s were obtained as a result of the frequency time analysis of seismic signals of more than 400 ray-paths in the region. For each cell of 2° × 2°, group velocity dispersion curves were determined and extended to 150 s by adding data from a larger scale tomographic study (Vdovin *et al*., Geophys. J. Int 136:324–340, 1999). Using, as independent a priori information, the available geological and geophysical data of the region, each dispersion curve has been inverted by the "hedgehog" non-linear procedure (Valyus, Determining seismic profiles from a set of observations (in Russian), Vychislitielnaya Seismologiya 4, 3–14. English translation: Computational Seismology (V.I. Keylis-Borok, ed.) 4:114–118, 1968), in order to compute a set of V_s versus depth models up to 300 km of depth. Because of the non-uniqueness of the solutions for each cell, a local smoothness optimization has been applied to the whole region in order to choose a three-dimensional model of V_s, satisfying this way the Occam's razor concept. Several known and some new main features of the Caribbean lithosphere and asthenosphere are shown on these models such as: the west directed subduction zone of the eastern Caribbean region with a clear mantle wedge between the Caribbean lithosphere and the subducted slab; the complex and asymmetric behavior of the crustal and lithospheric thickness in the Cayman ridge; the predominant oceanic crust in the region; the presence of continental type crust in Central America, and the South and North America plates; as well as the fact that the bottom of the upper asthenosphere gets shallower going from west to east.

Key words: S-wave velocity models, Caribbean region, Group velocities dispersion curves, Local smoothness optimization.

1. Introduction

The structure of the crust and upper mantle of the Caribbean region, located between the Pacific and Atlantic oceans and the North and South America plates (Fig. 1), has been studied by several authors. Regional studies (Dengo and Case, 1990; Van Der Hilst, 1990; Vdovin *et al*., 1999; Bassin *et al*., 2000; Chulick and Mooney, 2002; Ligorría and Molina, 1997; Moreno *et al*. 2002; Pindell and Kennan 2001; Gonzalez *et al*., 2007; Miller *et al*., 2009; Growdon *et al*., 2009; Magnani *et al*., 2009) and global studies (Laske and Masters, 1997; Montagner and Kennett, 1996; Mooney *et al*., 1998) show evidence of its complexity, which is characterized by continental and accretionary crust, subduction zones, rifts, and a predominantly oceanic crust.

Different models have been proposed to describe the origin and evolution of the Caribbean; some of the most representative models are summarized by Iturralde and Lidiak (2000). Recently, Pindell and Kennan (2009) formulate a comprehensive hypothesis about the evolution of the Caribbean lithosphere and its interaction with the American Cordillera, from Baja California to northern Peru, as well as its progressive relative motion to the North and South America plates.

Previous studies of the lithosphere–asthenosphere system in the Caribbean region have been made using geophysical data (i.e. Ten Brink *et al*., 2001, 2002), P-wave travel time tomography (Van Der Hilst, 1990), local studies of surface waves and receiver function analysis (Miller *et al*., 2009, Growdon *et al*., 2009, Magnani *et al*., 2009) and some regional surface waves dispersion analysis (Álvarez, 1977; Papazachos, 1964; Santo, 1967; Tarr, 1969).

Recently, with the installation of new broad band seismic stations in the Caribbean (USGS Caribbean Network), a significant amount of Rayleigh surface

[1] Centro Nacional de Investigaciones Sismológicas. Ministerio de Ciencia, Tecnología y Medio Ambiente, Santiago de Cuba, Cuba. E-mail: oleary@ictp.it; oleary@cenais.cu; leoalvar@chcenais.cu; bladimir@cenais.cu

[2] The "Abdus Salam" International Centre for Theoretical Physics, ESP section, SAND Group, Trieste, Italy. E-mail: panza@units.it

[3] Department of Geosciences (DiGeo), University of Trieste, Trieste, Italy.

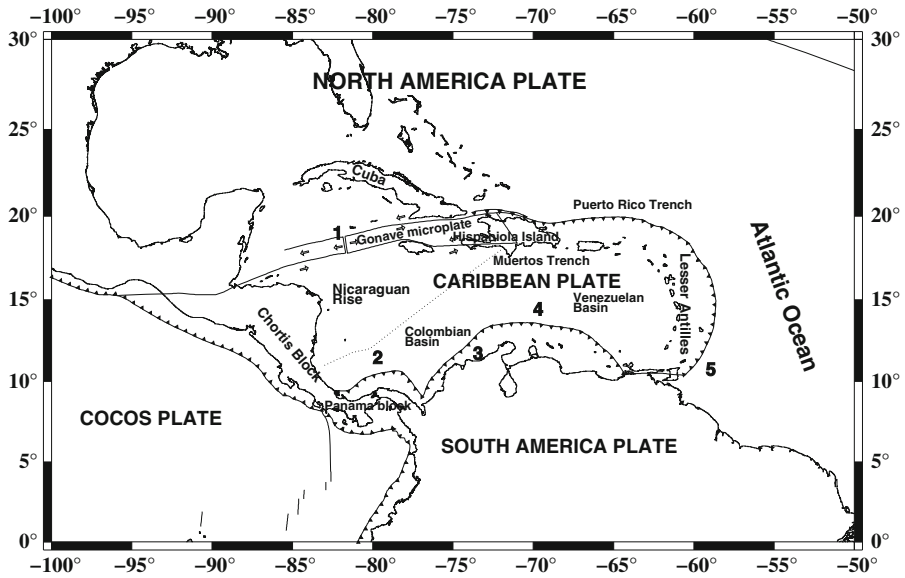

Figure 1
Schematic map of the Caribbean region (modified from González *et al.*, 2007). *1* Mid Cayman Spreading Center in the Cayman trough, *2* Northern Panama deformed belt, *3* South America deformed belt, *4* South Caribbean fold belt and *5* Barbados Prism)

waves have been recorded, which allow us to make a more detailed surface waves dispersion analysis for the whole region.

The purpose of this paper is to provide new information about the Rayleigh surface wave dispersion in the Caribbean region and to obtain the corresponding three-dimensional V_s model by a nonlinear inversion method, using the available knowledge about the lithosphere-asthenosphere system.

2. *Group velocity measurements and surface wave's tomography*

Two hundred-six new records of Rayleigh waves crossing the Caribbean region have been selected from the several thousands of waveforms recorded by the stations in the region (Table 1). The selected records, mainly of the USGS and FUNVISIS networks, fulfill the following conditions about the earthquake sources:

(a) Depth $h < 75$ km and magnitude $5.0 < M_S < 6.9$, to be able to record well defined Rayleigh surface waves at distances from 500 km to 2,000 km and to neglect finite-source effects.

(b) Latitude (north): 0°–35°, longitude (west): 40°–140°, whose ray-paths are crossing our study region.

(c) Mainly sampling the eastern zone of the Caribbean, where the spatial resolution of a previous study by González *et al.*, (2007) was the poorest.

The selected paths were added to those of the previous study by González *et al.*, (2007) (Fig. 2).

The frequency time analysis (FTAN, latest version) (Levshin *et al.*, 1972, 1992), has been used to determine the surface waves dispersion curves at periods from 10 to 40 s. The upper limit of this period range is imposed by the frequency response of the FUNVISIS seismic stations, the network with the highest number of stations in the southeastern Caribbean, which is equipped with Guralp CMG-40T seismometers.

The measurements errors of the group velocity values are determined as the average between the differences of group velocity values for at least five pairs of paths, where for each pair, the stations are the same and the distance between the epicenters is less than 0.3°. The results vary from 0.06 to 0.09 km/s and they are consistent with the ones in González *et al.*, (2007).

Table 1

Seismic stations used for this study

Code	Region	Latitude (N)	Longitude (W)	Height (m)	Network
RCCC	Rio Carpintero	19.999	75.696	100	SSSN
CCCC	Cascorro	21.200	77.766	150	SSSN
LMGC	Las Mercedes	20.064	77.005	220	SSSN
MOAC	Moa	20.660	74.960	120	SSSN
MASC	Maisi	20.175	74.231	320	SSSN
MGV	Manicaragua	22.110	79.980	300	SSSN
SOR	Soroa	22.784	83.008	206	SSSN
DWPF	Disney Wilderness Preserve	28.110	81.433	142	GSN
HKT	Hockley	29.950	95.833	415	GSN
SDV	Santo Domingo (Vzla)	8.886	70.633	1,580	GSN
TEIG	Tepich	20.226	88.276	69	GSN
SJG	San Juan	18.112	66.150	457	GSN
JTS	Juntas de Abangares	10.291	84.952	340	GSN
FUNV	El Llanito, Venezuela	10.470	66.810	875	FUN
CUPV	Cupira, Venezuela	10.057	65.788	668	FUN
MERV	Las Mercedes, Venezuela	9.251	66.297	156	FUN
CRUV	Carúpano, Venezuela	10.675	63.236	20	FUN
MONV	Montecano, Venezuela	11.955	69.971	170	FUN
ITEV	Isla los Testigos, Venezuela	11.355	63.132	13	FUN
IBAW	Isla La Blanquilla, Venezuela	11.823	64.577	100	FUN
ORIV	Oritupano, Venezuela	9.070	63.409	123	FUN
TURV	Turiamo, Venezuela	10.450	67.840	58	FUN
ORCV	Isla La Orchila	11.812	66.194	22	FUN
MPGF	Montagnes des Peres, Guyana F.	5.110	52.644	147	G
ANWB	Willy Bob, Antigua y Barbuda	17.669	61.786	39	CU
BBGH	Gun Hill, Barbados	13.143	59.559	180	CU
BCIP	Isla Barro Colorado, Panama	9.166	79.837	61	CU
BOA	Boaco, Nicaragua	12.482	85.718	550	INET
FDF	Fort de France	14.733	61.150	510	G
GRGR	Grenville, Grenada	12.132	61.654	195	CU
GRTK	Grand Turk, Turks and Caicos Islands	21.511	71.133	12	CU
GTBY	Guantanamo Bay, Cuba	19.927	75.111	79	CU
HDC	Heredia, Costa Rica	10.000	84.112	1,186	G
MTDJ	Mount Denham, Jamaica	18.226	77.534	925	CU
OTAV	Otavalo, Ecuador	0.2398	78.451	3,510	IU
SAML	Samuel, Brazil	8.949	63.183	120	IU
SDDR	Presa Sabenta, República Dominicana	18.982	71.288	589	CU
TGUH	Tegucigalpa, Honduras	14.057	87.273	0	CU
BBSR	St George's, Bermuda	32.371	64.696	30	IU

SSSN Cuban National Seismological Survey, *GSN* global seismic network, *FUN* Venezuelan Foundation of Seismological Research, *IU* global seismograph network (GSN-IRIS/USGS), *CU* Caribbean network (USGS), *G* GEOSCOPE, *INET* INETER, *XT* South Eastern Caribbean passive experiment

Using the tomographic procedure described by Ditmar and Yanovskaya (1987), Yanovskaya and Ditmar (1990), Wu and Levshin (1994), and Yanovskaya (1997), a new tomographic maps of the group velocity in the Caribbean were determined at periods from 10 to 40 s with 5 s intervals (Fig. 3). These maps are an improved and extended version of those obtained by Gonzalez *et al*., (2007) in the southeastern part of the Caribbean.

The lateral resolution of the tomographic study (Fig. 4), which is determined by the density of paths, is less than 500 km in the whole region, including the southeastern part of the Caribbean and the Lesser Antilles, except for the period of 10 s. The stretching parameter ε (Fig. 5), that indicates the dominant orientation of the paths, are evidence of a satisfactory uniform spatial distribution of the paths in the study area.

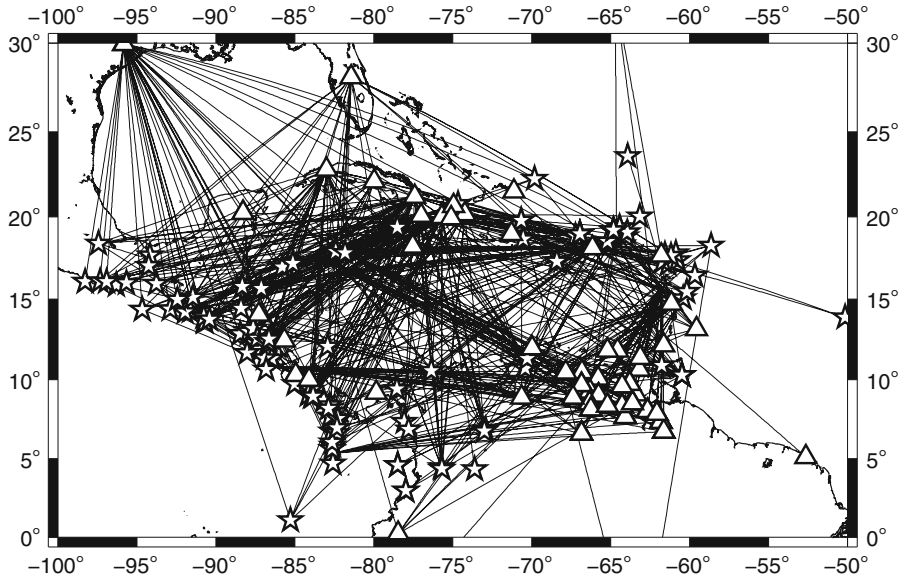

Figure 2
Epicenters (*stars*), stations (*triangles*) and seismic paths selected for surface-wave tomography

3. *Non-Linear Inversion and Local Smoothness Optimization*

A group velocity dispersion curve in the period range from 10 to 40 s (at intervals of 5 s) for each cell of 2° × 2° has been determined for the region of study as a result of the tomographic maps, (see Appendix 1).

These dispersion curves are the input for the non-linear inversion procedure "hedgehog" (Valyus, 1968) used for determining V_s versus depth models.

For each cell, the values of the parameters describing the sedimentary layers, and in some cases down to the upper crust, were fixed according to the a priori information from previous studies, like Bassin *et al*. (2000), Chulick and Mooney (2002), Ligorría and Molina (1997), Magnani *et al*. (2009), Miller *et al*. (2009), Moreno *et al*. (2002) and Moreno (2003). Where the a priori information was less detailed or absent, data from global models of the crust (Mooney *et al*., 1998), sediments (Laske and Masters, 1997) and bathymetry (Smith and Sandwell, 1997) were used.

In the inversion procedure, the lateral resolving power of the dispersion data, determined by the density and orientation of the paths, is improved by the a priori independent geological and geophysical information about the shallow crustal structure (Chimera *et al*., 2003; Pontevivo and Panza, 2006).

The study area has been previously sampled by Vdovin *et al*. (1999) with a broader-than-our regional scale tomography, using path lengths longer than 4,500 km. The density of these paths is lower, the azimuthal distribution is less uniform than in our study, and should be taken into account that the determination of geologically meaningful group velocities for periods less than 30 s is questionable over distances of several thousands of km. On the contrary, the group velocity tomographic results of Vdovin *et al*. (1999) can be readily used to extend our dispersion relations to longer periods, in the range of 60 to 150 s, because at these longer periods the dispersion curves are mainly controlled by deep structural features. The depth sensitivity of the group velocity is expressed through its partial derivative with respect to S-wave velocity as a function of the depth. In Fig. 6 it is shown at some inverted periods.

The measurement errors of the group velocity values were taken as the experimental error associated to the inversion results. However, for the Vdovin *et al*. (1999) data, to be conservative, as the experimental error associated at each period were used the same values determined at the shorter periods, and

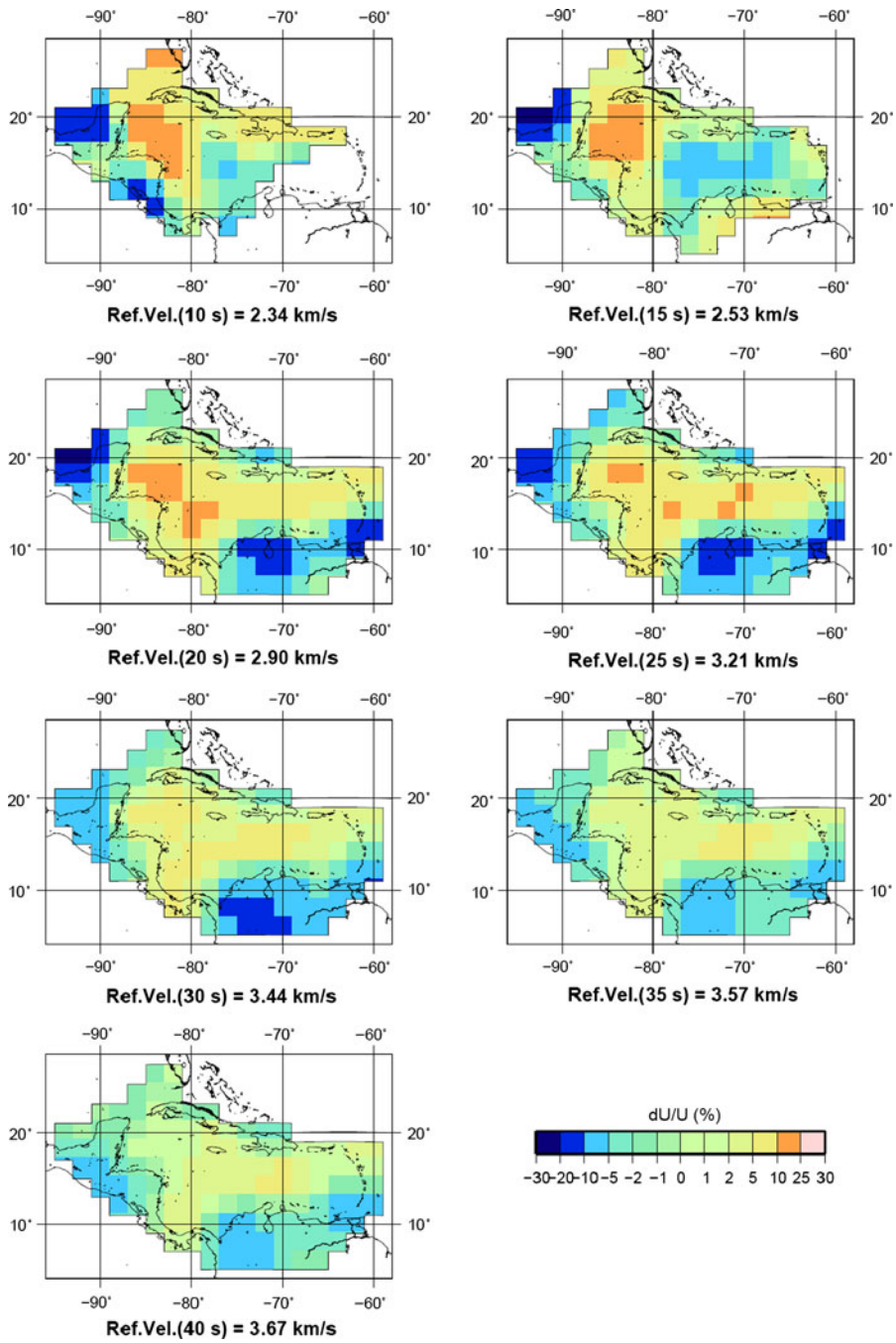

Figure 3
Rayleigh waves group velocity tomographic maps at different periods (10–40 s) shown as percent deviation from the average reference velocity at each period (Ref. Vel.)

not the smaller values determined by VDOVIN *et al.* (1999) along much longer profiles.

The models were composed by four surface layers with fixed parameters and five deeper layers with parameters to be inverted. Because of the depth resolution of the dispersion curves (up to 150 s) (Fig. 6), only the layers at depth up to 300 km were inverted. For greater depths the models were fixed

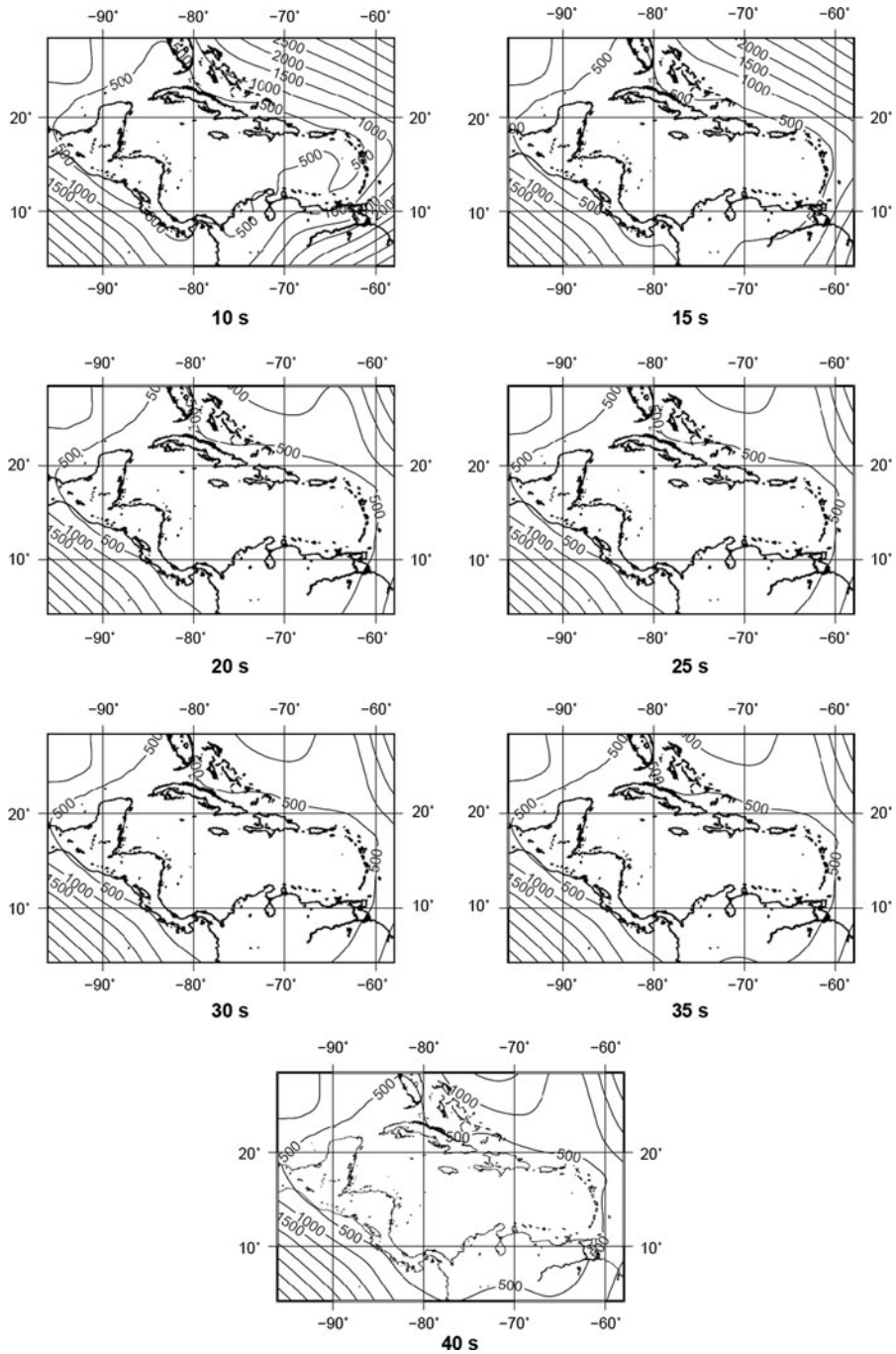

Figure 4
Map of lateral resolution (km) at different periods (10–40 s)

from Du *et al.* (1998), which is a compilation of global models at these depths and covers the Tyrrhenian region, where a west directed subduction zone is also present.

The inverted parameters for each of the five inverted layers were their thickness and S-wave velocities. Because of the low sensitivity of Rayleigh waves to P-wave at the inverted depths, P-wave

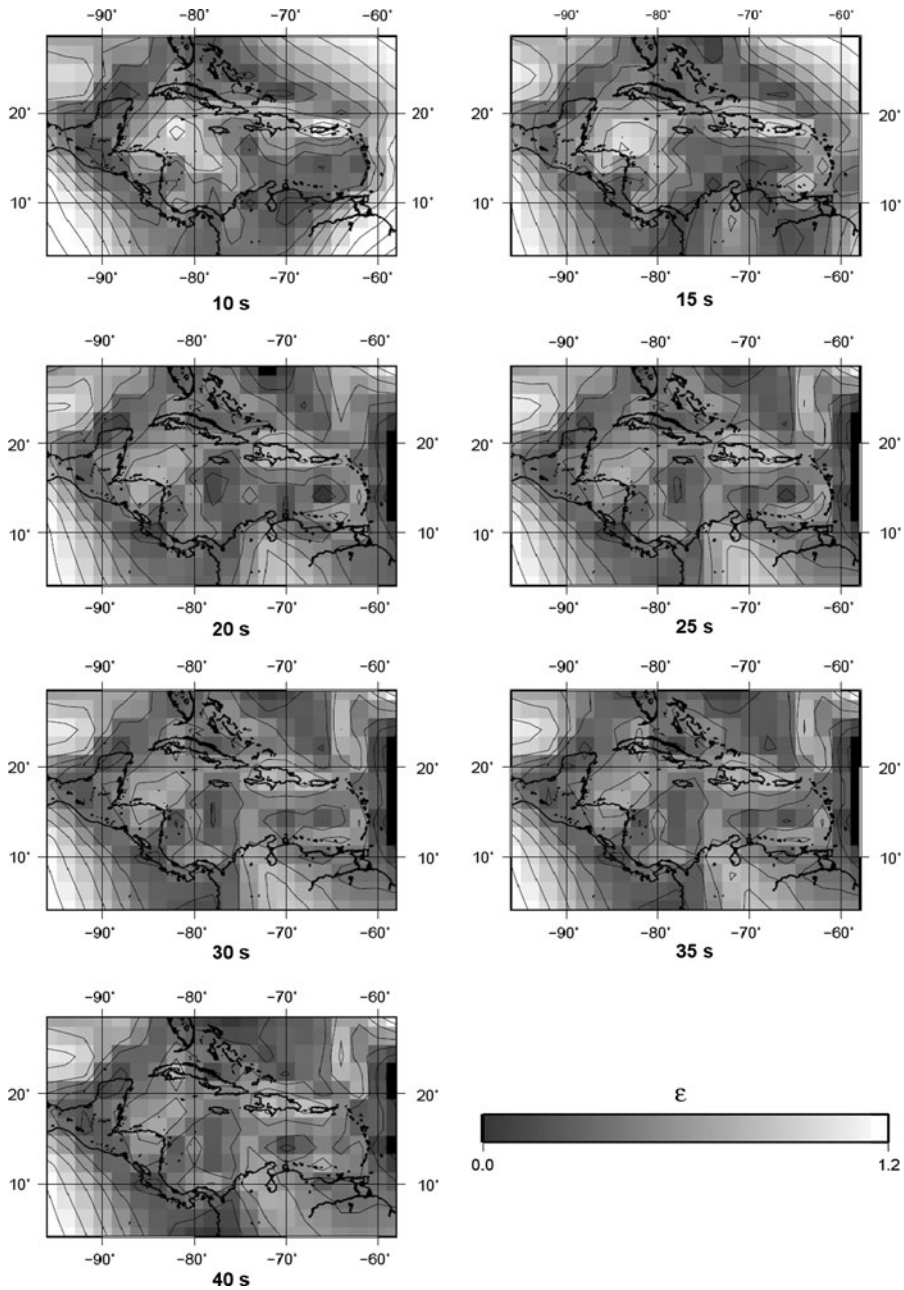

Figure 5
Maps of the azimuthal resolution, $\varepsilon = 2b/a$, at different periods (10–40 s). Small values of ε ($\leq$0.5) indicate that the obtained solution is locally smoothed over an area of the same size in all directions, large values ($\varepsilon \geq 1$) indicate that a preferred orientation of the paths exists

velocities were calculated from the relationship $Vp/V_s = \sqrt{3}$, assuming Poissonian solids. The density was fixed at the beginning of the inversion from the Nafe and Drake relationship (Grant and West, 1965; Fowler, 1995), due to its low influence on the final results (e.g. see Panza, 1981).

The parameterization of the input data and the adequate step ΔP_i were defined following the procedure described by Panza (1981), and using the codes developed by Urban *et al.* (1993) for the analytical determination of the partial derivatives of the dispersion relations with respect to the

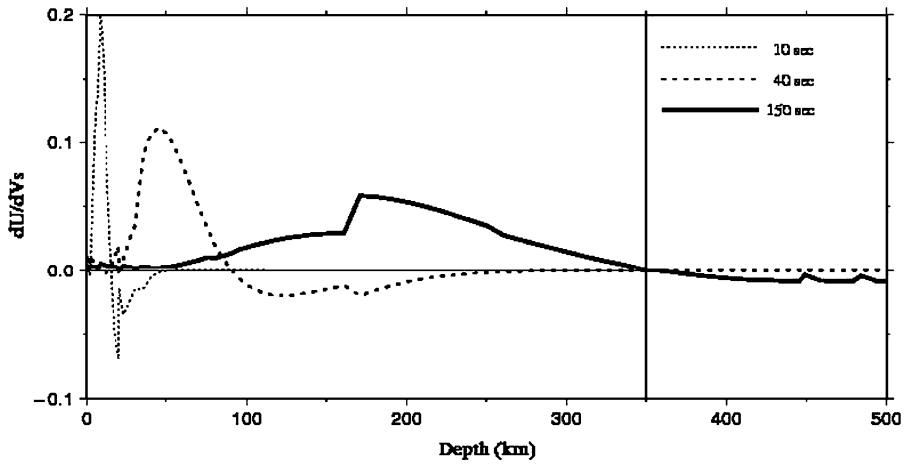

Figure 6
An example of partial derivative of the Rayleigh wave group velocity with respect to S-wave velocity as a function of depth at periods of 10, 40 and 150 s. The *solid line* corresponds to the added data of Vdovin *et al.* (1999)

structural parameters. The step ΔP_i is a measure of the uncertainty (resolution) for each inverted parameter and implies, that one solution of the inversion differ from the others in at least $\pm\Delta P_i$ for one parameter P_i.

The "hedgehog" inversion procedure (Valyus, 1968) is a Monte Carlo search, which finds in a fully non-linear form, the V_s versus depth models consistent with the dispersion curves and optimized with the use of a guided method that remembers the results of the previous trials. For each model of the searching process, which are several thousand, a theoretical dispersion curve is calculated. As solutions of the inversion (Biswas, 1974; Panza, 1981) are considered those models for which, at each period, the difference between the theoretical and the experimental values is less than the measurement error, and the rms value of the differences along the entire dispersion curve is less than 60% of the average experimental error. The results of this procedure yield several models (between 10 and 30 models for each cell) keeping the a priori information used to constrain their parameters. An example of this procedure is presented in Fig. 7.

A set of models which are solutions of the inversion procedure, in agreement with the available geophysical and geological data, is obtained for each cell and their number varies from 10 to 30 models.

In previous studies several criteria have been applied to select from the set of solutions one model for each cell. Some of them are based on choosing the median model of all the solutions (Shapiro and Ritzwoller, 2002) as well as choosing the solution according to the rms minimum, or as close as possible to the average value of the rms. of the all solutions (Gonzalez *et al.*, 2007).

Other optimization methods to select a model for each cell are described by Boyadzhiev *et al.* (2008). These methods are based on the concept of William of Occam's razor: "it is vain to do with more what can be done with less".

In our case, considering that all the models are consistent with the geological and geophysical information, we choose for the selection of one model for each cell the local smoothness optimization method (LSO) (Boyadzhiev *et al.*, 2008) not only because it is very fast, but in general it looks for the representative solution in the area from one cell to the other, following the criteria of maximum local smoothness (only between neighboring cells), which is quite appropriate for a region like the Caribbean, with very large heterogeneities.

As a final result, a model of V_s up to 300 km of depth in 85 (2° × 2°) cells is obtained (see Figs. 8, 9, 10 and Appendix 2), representing the first approximation, at this level of detail, of the structure of the lithosphere-asthenosphere system in the Caribbean region.

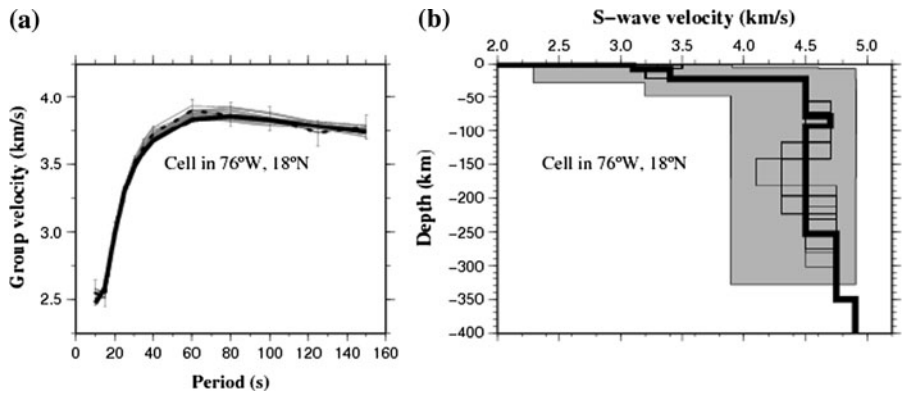

Figure 7
An example of selection of the solution (corresponds to cell in 76°W, 18°N): **a** experimental dispersion curve (*dashed line*), synthetic dispersion curves of acceptable models (*thin gray lines*) and dispersion curve of chosen model (*thick line*); **b** acceptable models by non-linear inversion (*thin lines*) and chosen model by LSO (*thick line*)

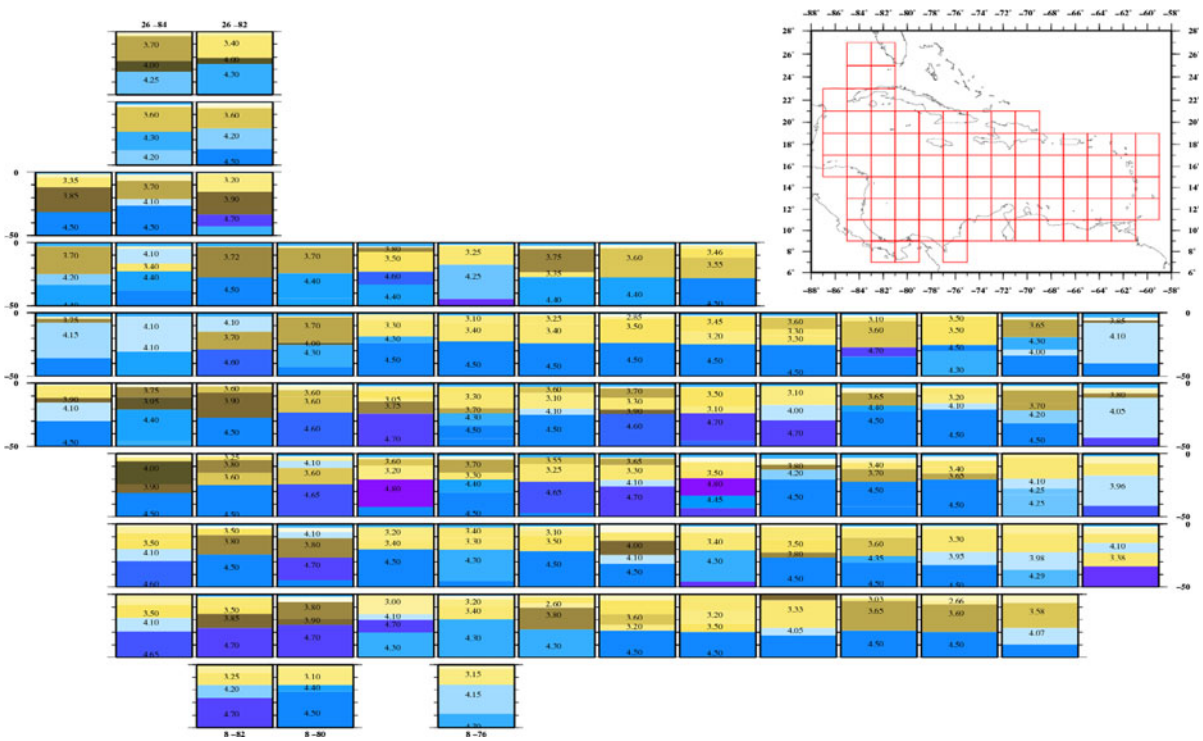

Figure 8
V_s versus depth models up to 50 km. The numbers correspond to the V_s velocities of the selected solution by LSO and their ranges of variability are in Appendix 2

4. Results and Discussion

The tomographic maps cover the southeastern part of the Caribbean and its subduction zone, extending the area covered by the previous study of Gonzalez *et al*., (2007).

At the most southeastern part of the study area, a relatively low group velocity at periods from 20 to 40 s is found (Fig. 3), which is consistent with the presence of the subduction zone and the older part of the Caribbean crust (Pindell and Kennan, 2009). In the southern part, at some periods, the group velocity

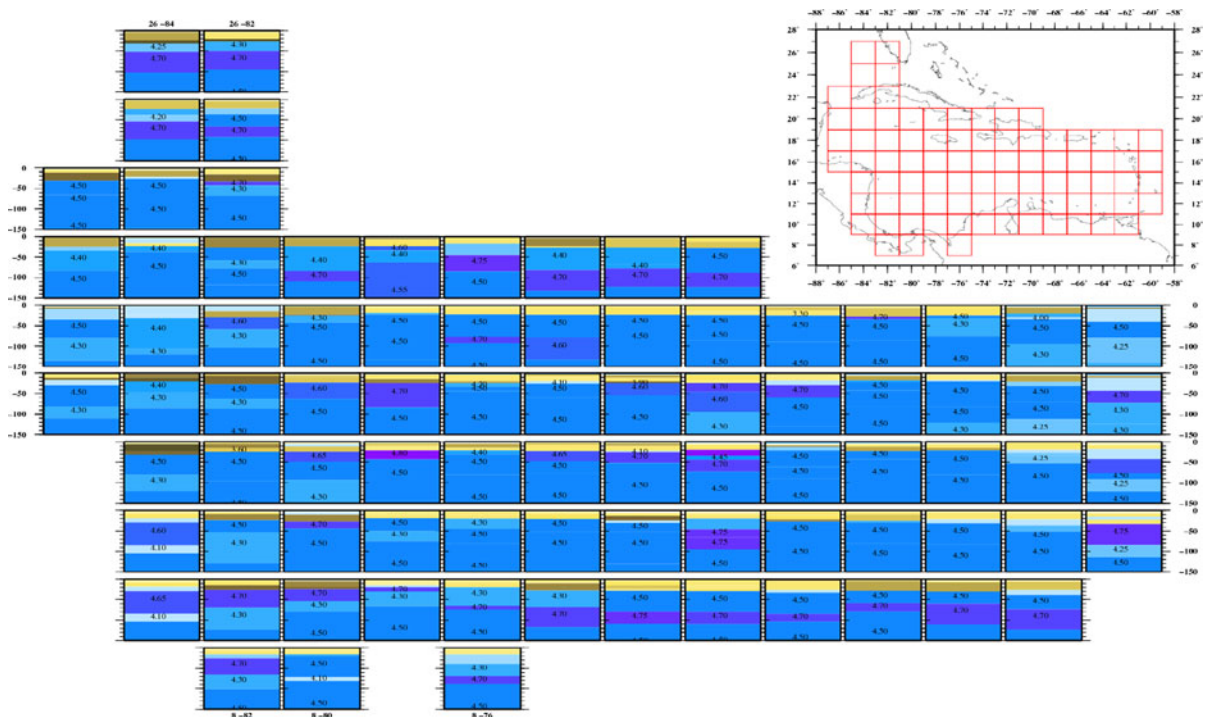

Figure 9
V_s versus depth models up to 150 km

is as low as in the northern part of the South America plate, where the crust is mainly continental (Dengo and Case, 1990; Pindell and Kennan, 2001). Such a situation could be explained by the known contact between the accretionary wedge (the Barbados prism), with the right-lateral transpression and clockwise rotations of the thrust sheets in the southern part of a West-directed subduction zone (Doglioni *et al*., 1999).

The V_s structure of the Caribbean is shown in Figs. 8, 9 and 10 down to 50, 150 and 300 km of depth, respectively. For the uppermost 50 km (Fig. 8), in the northern part of the South America Plate and the south Caribbean fold belt (cells in 74°–62°W, 10°N), there is evidence of a predominant presence of continental crust $\sim$30 km thick (Dengo and Case, 1990), while in the most northeastern part of the region (cells in 60°W, 16°–18°N), a typical oceanic crust is present, which could belong to the younger Atlantic crust.

The results also reveal a well defined thick crust in some known typical continental crust areas, like in the northeast of Yucatan in Central America (cells in 86°W, 22°N), the Chortis blocks (cell in 84°W,14°N) (Dengo and Case, 1990), and the western part of Cuba (cells in 82°W, 20°–22°N) (Tenreyro *et al*., 1994). To the east of the Chortis block (cells in 82°–74°W, 14°N; 74°–70°W, 16°N and 70°W, 18°N) mostly coinciding with the Hess Escarpment (Pindell and Kennan, 2009), relatively high velocities in the upper crust are found.

In Fig. 8 is shown evidence of other main features of the Caribbean crust, like the Mid-Cayman spreading center (MCSC) (cell in 86°–82°W, 18°N), with very thin sedimentary layers overlaying the uppermost lithospheric mantle. Along the profile A–A′ of Fig. 11, mostly coinciding with the MCSC and the Cayman trough, the thinnest crust is found to the west of the ridge, in good agreement with previous studies (Ten Brink *et al*., 2001), while to the east, the crust is accreted by new material rising from the ridge. A relatively shallower basement in the easternmost part of Cayman trough (cells in 80°–78°W, 18°N, see also Fig. 8) is also consistent with previous

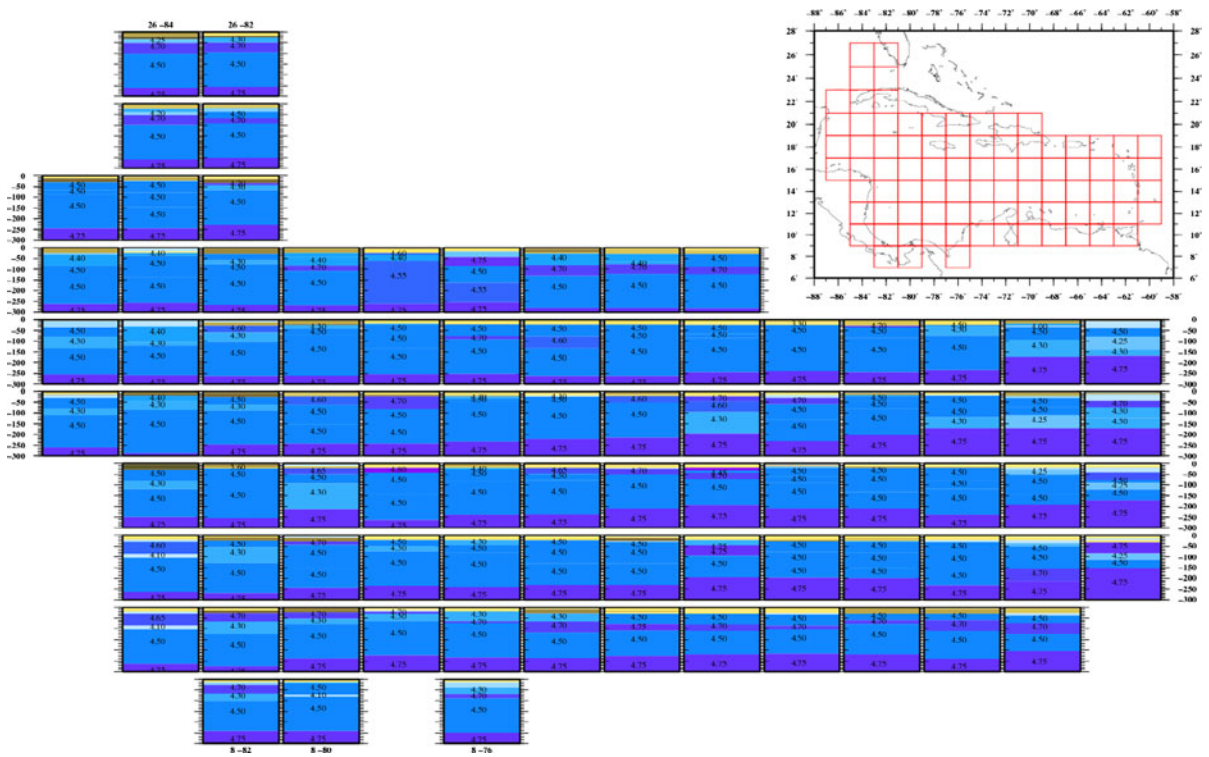

Figure 10
V_s versus depth models up to 300 km

results from gravity field modeling (Ten Brink *et al.*, 2002). The lithosphere is thicker on the western side of the MCSC than in the eastern side, which is in good agreement with the global asymmetric pattern of the deep part of the ridges shown by Panza *et al.* (2010).

Coincidentally with the region where a lithospheric slab of the Atlantic is being subducted under the Caribbean Plate (Pindell and Kennan, 2009) (cells 64°W, 18°N; 62°W, from 10° to 18°N and 60°W, from 12° to 18°N and profile B–B′ of Fig. 11), low velocities characterize the upper mantle and mark the presence of the mantle wedge, which is located between the upper and lower plate of the west directed subduction process (Doglioni *et al.*, 2009).

The crustal thickness in the western part of the Caribbean plate (cells in 80°–70°W, 12°–18°N in Fig. 8) ranges from 20 to 25 km, while in the east (cells in 68°–62°W, 14°–16°N) the crust is thinner and some low velocity values are present in the upper mantle (see also profile B–B′ of Fig. 11). Such features are consistent with the presence of a wide back arc basin (Pindell and Kennan, 2001) and the rejuvenation, from west to east, of the Caribbean plate due to the eastward retreat of the subduction zone (Doglioni *et al.*, 2007).

The lithospheric thicknesses are well defined in cells located along the major strike-slip fault zones, and the velocities for the deepest lithospheric layers are, in general, relatively high. In the most southern part (cells from 74° to 62°W, 10°N), i.e. in the South America Plate and the southern Caribbean fold belt, the lithospheric thickness varies between 80 and 120 km. To the northwestern side of this fault system, the underthrusting of the South American plate by the Caribbean slab [the so-called Caribbean Large Igneous Province CLIP (Miller *et al.*, 2009)], is evident (in cells 72°W, 14°N and 70°W, from 12° to 14°N), as can be seen in Figs. 7, 8 and profile B–B′ of Fig. 11.

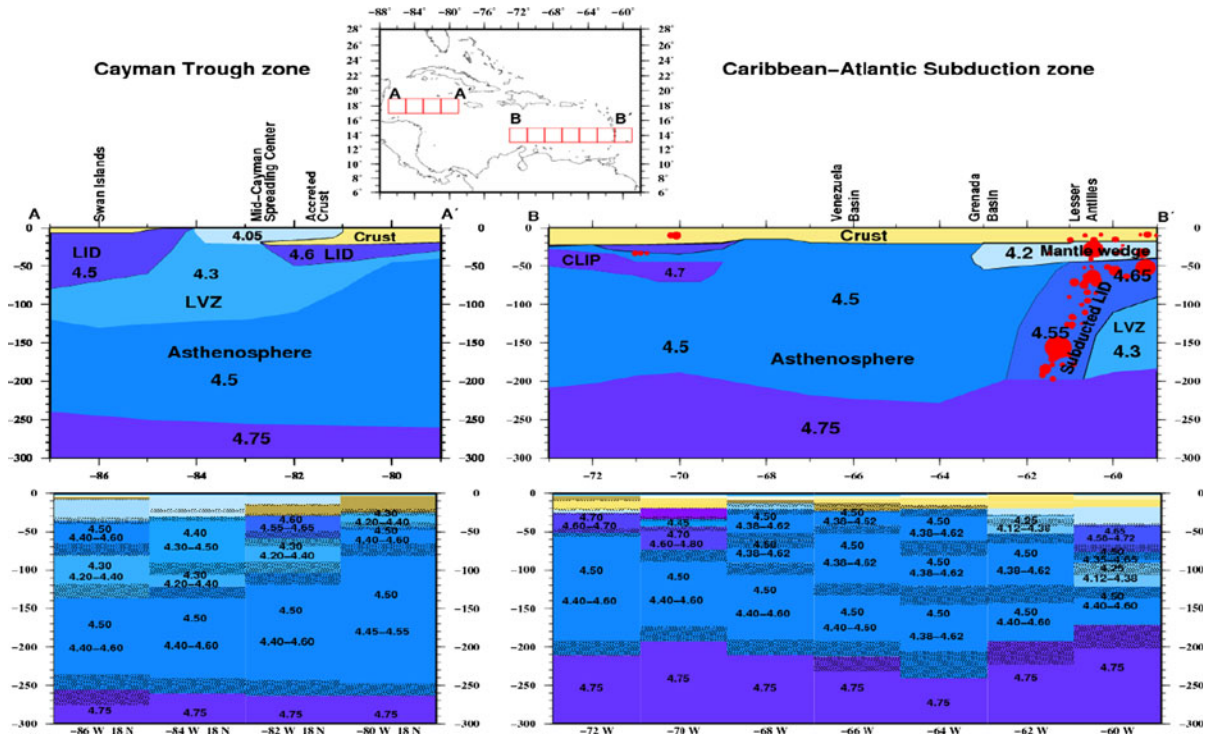

Figure 11

Profiles V_s versus depth along the Cayman trough and the Caribbean—Atlantic subduction zone with the corresponding schematic interpretative cartoons. (*CLIP* Caribbean large igneous Province, *LVZ* low velocity zone; red dots are earthquake hypocenters of magnitude $M > 5.0$ from NEIC). The V_s values and its ranges of uncertainty are included in the profiles; the error on thickness is represented by *texture*. In the interpretation some representative values of V_s are given that fall within the uncertainty range

At the boundary between the North America Plate and the Caribbean Plate (cells 82°W, 18°N and from 80°W to 70°W, 20°N) the lithospheric thickness is significantly increased at the contact between the Gonave Microplate and Hispaniola Island (in cells from 76°W to 74°W, 20°N). This lithospheric thickening from 80 km to more than 130 km is related to the presence of several major active tectonic structures on Hispaniola Island, which accommodate the relative motion between the Caribbean, the North America Plate and the Gonave Microplate (Mann et al. 1998; Mann 2002; Pindell and Kennan, 2009).

In the Caribbean, the bottom of the upper asthenosphere, within which sometimes a well developed low velocity zone is present, gets shallower from west to east, from around 250 km in the east of Central America to about 160 km in the Lesser Antilles (Fig. 10).

5. Conclusions

The obtained three-dimensional V_s versus depth model of the Caribbean region is consistent with the available knowledge about the lithosphere-asthenosphere system, and provides new information about the areas with none or poor studies at this resolution level.

The 1-D models of V_s versus depth determined for each cell by a non-linear inversion were processed with a LSO procedure, giving a 3-D structure, with its uncertainties, of the Caribbean down to a depth of about 300 km. In this model some important features of the Caribbean crust are well distinguished, like the diffused presence of the oceanic crust in the region, the thick continental crust in the South American plate and others isolated regions in Central America, as well as the rejuvenation, from west to east, of the crust of the Caribbean Plate. In the major strike-slip

fault zones (between the North America plate, South America plate and the Caribbean Plate) the lithospheric thickness ranges from 80 to 130 km with a relatively high velocity values in the lower lithosphere. The crust and lithosphere thickness to the west and east of the Mid-Cayman spreading center are asymmetric, the crust is thinner to the west while their corresponding lithosphere is thicker. To the east of the MCSC the new mantle material accreted the existing crust, while from more than 200 km east of the rise the crust becomes thinner. Several cells, mainly belonging to the Hess Escarpment, have high velocity layers in the upper crust, while more to the east, the underthrusting of the South American plate by the Caribbean Plate is well defined. In the Caribbean Plate, going from west to east, the top of the lower asthenosphere gets shallower from around 250 km deep in the east of Central America, to about 160 km in the subduction zone.

The 3-D model proposed by this study is an opportunity to improve the geodynamic knowledge of the Caribbean Plate. The result has important implication for several seismological applications, like waveform modeling, earthquake location, moment tensor inversion, and others.

Acknowledgments

The authors express thanks to Anatoli L. Levshin from the University of Colorado, for kindly providing us with the long-period group velocities available at CIEI, University of Colorado at Boulder and the staff of the Earth Science Department of the University of Trieste for all their help and facilities, especially to Enrico Brandmayr for the use of the LSO code. The authors also want to express their thanks to Julio Garcia, from National Institute of Oceanography, Geophysics and Seismology (OGS) of Italy and to Prof. Carlo Doglioni (Dipartimento di Scienze della Terra, Università Sapienza di Roma) for their help in the geological interpretation of results, as well as Dr. Margaret Wiggins-Grandison, former Director of the Jamaica Seismograph Network and Dr. Jorge del Pino Boytel, former researcher of the National Centre for Seismological Research of Cuba for the grammatical corrections. The present work was done with the financial support of the Associate Scheme, TRIL Programs and ESP (SAND group) Section of the "Abdus Salam" International Centre for Theoretical Physics, the Ministry of Science, Technology and Environment of Cuba through projects PNCB 020/04, PTCT 17-05 and PTSCu 08-8, as well as founded by the Italian MIUR Cofin-2001 (2001045878_007), Cofin-2002 (2002047575_002), the Italian MIUR Cofin-2001 (2001045878_007), Cofin-2002 (2002047575_002), PRIN2008, the Italian Programma Nazionale di Ricerche in Antartide (PNRA) 2004-2006, project 2.7-2.8 ("Sismologia a larga banda nella regione del Mare di Scotia e suo utilizzo per lo studio della geodinamica dellalitosfera") and project: Sismologia a larga banda, geodinamica e strutture litosferiche nella regione del Mare di Scotia (2009/A2.17) and the UNESCO through Project UNESCO/IGCP 487 and from ICTP through Network NET-58..

Appendix 1

See Table 2.

Table 2

Values of group velocity dispersion curves for each cell

Period T (s)	Group velocity (km/s)												
	W-62.0 N10.0	W-64.0 N10.0	W-66.0 N10.0	W-68.0 N10.0	W-70.0 N10.0	W-72.0 N10.0	W-74.0 N10.0	W-76.0 N10.0	W-78.0 N10.0	W-80.0 N10.0	W-82.0 N10.0	W-84.0 N10.0	W-60.0 N12.0
10							2.280	2.300	2.285	2.470	2.350	2.070	
15			2.740	2.790	2.620	2.605	2.620	2.560	2.505	2.750	2.740	2.595	2.630
20	2.570	2.680	2.730	2.715	2.635	2.560	2.620	2.760	3.015	3.105	3.050	3.015	2.620
25	2.785	2.895	3.015	2.950	2.865	2.805	2.855	2.945	3.270	3.460	3.480	3.310	2.795
30	3.115	3.200	3.310	3.290	3.205	3.150	3.120	3.145	3.405	3.585	3.715	3.630	3.200
35	3.270	3.360	3.500	3.460	3.395	3.325	3.300	3.305	3.505	3.695	3.785	3.665	3.390
40	3.390	3.455	3.550	3.565	3.540	3.490	3.430	3.440	3.625	3.740	3.825	3.665	3.510
60	3.815	3.840	3.855	3.855	3.840	3.825	3.810	3.795	3.800	3.800	3.785	3.785	3.745
80	3.800	3.830	3.855	3.870	3.870	3.860	3.850	3.835	3.830	3.815	3.795	3.795	3.730
100	3.810	3.835	3.860	3.870	3.875	3.865	3.840	3.815	3.800	3.780	3.770	3.770	3.735
125	3.845	3.840	3.835	3.830	3.825	3.810	3.795	3.780	3.760	3.730	3.710	3.705	3.835
150	3.790	3.790	3.795	3.790	3.785	3.780	3.770	3.755	3.740	3.720	3.705	3.710	3.775

Period T (s)	Group velocity (km/s)												
	W-62.0 N12.0	W-64.0 N12.0	W-66.0 N12.0	W-68.0 N12.0	W-70.0 N12.0	W-72.0 N12.0	W-74.0 N12.0	W-76.0 N12.0	W-78.0 N12.0	W-80.0 N12.0	W-82.0 N12.0	W-84.0 N12.0	W-60.0 N14.0
10							2.275	2.305	2.285	2.550	2.435	2.175	
15	2.515	2.510	2.580	2.545	2.475	2.440	2.470	2.485	2.455	2.640	2.650	2.570	2.655
20	2.565	2.745	2.950	2.980	2.895	2.790	2.870	3.010	3.315	3.360	3.230	3.045	2.820
25	2.900	3.060	3.210	3.175	3.090	3.085	3.190	3.230	3.470	3.570	3.485	3.295	3.000
30	3.155	3.295	3.455	3.400	3.300	3.310	3.380	3.390	3.575	3.675	3.690	3.555	3.315
35	3.310	3.420	3.575	3.550	3.480	3.490	3.510	3.515	3.645	3.745	3.745	3.610	3.475
40	3.420	3.485	3.585	3.650	3.650	3.645	3.635	3.625	3.745	3.815	3.795	3.655	3.620
60	3.780	3.815	3.840	3.850	3.845	3.850	3.850	3.850	3.830	3.810	3.790	3.780	3.715
80	3.760	3.780	3.810	3.835	3.845	3.860	3.865	3.860	3.850	3.840	3.825	3.800	3.700
100	3.765	3.795	3.820	3.835	3.845	3.845	3.840	3.825	3.805	3.790	3.775	3.765	3.705
125	3.835	3.825	3.820	3.815	3.810	3.790	3.775	3.760	3.750	3.735	3.710	3.690	3.825
150	3.770	3.765	3.765	3.765	3.770	3.765	3.760	3.755	3.745	3.730	3.720	3.710	3.780

Period T (s)	Group velocity (km/s)												
	W-62.0 N14.0	W-64.0 N14.0	W-66.0 N14.0	W-68.0 N14.0	W-70.0 N14.0	W-72.0 N14.0	W-74.0 N14.0	W-76.0 N14.0	W-78.0 N14.0	W-80.0 N14.0	W-82.0 N14.0	W-84.0 N14.0	W-60.0 N16.0
10						2.300	2.270	2.235	2.150	2.445	2.740	2.565	
15	2.525	2.545	2.525	2.405	2.435	2.430	2.420	2.400	2.290	2.545	2.765	2.875	2.720
20	2.960	3.020	3.065	3.120	3.225	3.280	3.260	3.235	3.395	3.310	3.225	3.095	3.015
25	3.210	3.340	3.390	3.345	3.450	3.630	3.615	3.480	3.680	3.600	3.445	3.325	3.240
30	3.390	3.490	3.585	3.565	3.655	3.755	3.705	3.625	3.705	3.710	3.630	3.495	3.445
35	3.525	3.585	3.705	3.715	3.785	3.840	3.810	3.750	3.795	3.785	3.710	3.590	3.540
40	3.645	3.630	3.700	3.800	3.890	3.915	3.890	3.815	3.865	3.870	3.745	3.640	3.690

Table 2

continued

Period T (s)	Group velocity (km/s)												
	W-62.0 N14.0	W-64.0 N14.0	W-66.0 N14.0	W-68.0 N14.0	W-70.0 N14.0	W-72.0 N14.0	W-74.0 N14.0	W-76.0 N14.0	W-78.0 N14.0	W-80.0 N14.0	W-82.0 N14.0	W-84.0 N14.0	W-60.0 N16.0
60	3.755	3.790	3.820	3.845	3.865	3.885	3.885	3.870	3.855	3.840	3.830	3.810	3.690
80	3.735	3.760	3.785	3.805	3.835	3.855	3.865	3.865	3.860	3.855	3.850	3.840	3.680
100	3.740	3.770	3.790	3.810	3.820	3.830	3.830	3.825	3.810	3.800	3.790	3.785	3.680
125	3.815	3.805	3.805	3.795	3.785	3.775	3.760	3.755	3.750	3.740	3.720	3.700	3.810
150	3.775	3.770	3.765	3.760	3.755	3.750	3.750	3.750	3.745	3.735	3.720	3.705	3.775

Period T (s)	Group velocity (km/s)												
	W-62.0 N16.0	W-64.0 N16.0	W-66.0 N16.0	W-68.0 N16.0	W-70.0 N16.0	W-72.0 N16.0	W-74.0 N16.0	W-76.0 N16.0	W-78.0 N16.0	W-80.0 N16.0	W-82.0 N16.0	W-84.0 N16.0	W-86.0 N16.0
10				2.260	2.305	2.335	2.395	2.320	2.230	2.630	2.865	2.850	2.520
15	2.620	2.610	2.470	2.390	2.485	2.425	2.385	2.435	2.480	2.820	2.965	3.090	2.820
20	3.065	3.170	3.180	3.265	3.400	3.325	3.185	3.065	3.130	3.185	3.230	3.415	3.225
25	3.320	3.445	3.485	3.610	3.765	3.650	3.480	3.330	3.445	3.440	3.490	3.620	3.460
30	3.465	3.590	3.675	3.800	3.880	3.790	3.665	3.565	3.585	3.575	3.610	3.625	3.600
35	3.555	3.665	3.745	3.870	3.935	3.870	3.765	3.730	3.730	3.670	3.650	3.620	3.660
40	3.670	3.690	3.745	3.925	3.975	3.925	3.830	3.810	3.820	3.745	3.670	3.630	3.655
60	3.735	3.780	3.810	3.845	3.885	3.900	3.895	3.890	3.875	3.865	3.855	3.850	3.825
80	3.725	3.755	3.780	3.800	3.825	3.845	3.860	3.865	3.870	3.870	3.870	3.865	3.845
100	3.720	3.750	3.775	3.795	3.810	3.825	3.830	3.830	3.820	3.810	3.805	3.795	3.785
125	3.795	3.795	3.785	3.775	3.770	3.760	3.755	3.750	3.740	3.730	3.720	3.710	3.705
150	3.780	3.780	3.780	3.775	3.770	3.765	3.760	3.750	3.740	3.725	3.710	3.690	3.685

Period T (s)	Group velocity (km/s)											
	W-60.0 N18.0	W-62.0 N18.0	W-64.0 N18.0	W-66.0 N18.0	W-68.0 N18.0	W-70.0 N18.0	W-72.0 N18.0	W-74.0 N18.0	W-76.0 N18.0	W-78.0 N18.0	W-80.0 N18.0	W-82.0 N18.0	W-84.0 N18.0
10			2.515	2.500	2.495	2.540	2.585	2.635	2.510	2.315	2.585	2.760	2.875
15	2.780	2.730	2.660	2.445	2.405	2.565	2.620	2.640	2.535	2.510	2.805	3.040	3.225
20	3.175	3.100	3.015	2.975	2.910	2.975	3.050	3.105	3.070	3.125	3.280	3.415	3.580
25	3.425	3.450	3.325	3.240	3.235	3.295	3.340	3.365	3.385	3.430	3.555	3.675	3.730
30	3.600	3.610	3.510	3.435	3.450	3.470	3.520	3.570	3.595	3.605	3.670	3.785	3.730
35	3.695	3.700	3.630	3.545	3.545	3.565	3.610	3.655	3.720	3.745	3.745	3.770	3.730
40	3.790	3.770	3.710	3.660	3.625	3.650	3.655	3.690	3.760	3.810	3.810	3.760	3.745
60	3.660	3.715	3.760	3.805	3.850	3.875	3.890	3.900	3.905	3.895	3.885	3.875	3.870
80	3.650	3.705	3.745	3.780	3.810	3.830	3.840	3.855	3.865	3.880	3.885	3.885	3.885
100	3.650	3.700	3.740	3.770	3.795	3.815	3.825	3.835	3.840	3.835	3.830	3.825	3.815
125	3.800	3.790	3.775	3.765	3.755	3.745	3.745	3.740	3.735	3.735	3.740	3.740	3.735
150	3.780	3.770	3.775	3.780	3.785	3.790	3.790	3.785	3.780	3.765	3.745	3.725	3.700

Table 2

continued

Period T (s)	Group velocity (km/s)												
	W-86.0 N18.0	W-70.0 N20.0	W-72.0 N20.0	W-74.0 N20.0	W-76.0 N20.0	W-78.0 N20.0	W-80.0 N20.0	W-82.0 N20.0	W-84.0 N20.0	W-86.0 N20.0	W-82.0 N22.0	W-84.0 N22.0	W-86.0 N22.0
10	2.730	2.610	2.525	2.485	2.425	2.375	2.545	2.560	2.780	2.675	2.485	2.455	2.560
15	3.165	2.630	2.600	2.575	2.595	2.690	2.830	3.020	3.020	2.810	2.730	2.660	2.770
20	3.480	2.830	2.780	2.835	2.955	3.100	3.090	3.105	3.155	3.055	2.955	2.970	2.995
25	3.630	3.040	3.040	3.120	3.320	3.380	3.360	3.460	3.545	3.420	3.240	3.290	3.215
30	3.645	3.320	3.300	3.380	3.550	3.550	3.515	3.655	3.665	3.555	3.555	3.555	3.415
35	3.695	3.445	3.420	3.525	3.700	3.720	3.630	3.675	3.700	3.625	3.635	3.660	3.530
40	3.725	3.575	3.545	3.625	3.770	3.825	3.670	3.665	3.720	3.675	3.675	3.730	3.635
60	3.860	3.855	3.875	3.885	3.895	3.900	3.895	3.885	3.880	3.870	3.895	3.885	3.875
80	3.875	3.825	3.840	3.845	3.855	3.875	3.885	3.895	3.895	3.890	3.890	3.895	3.890
100	3.805	3.810	3.830	3.840	3.840	3.850	3.855	3.850	3.845	3.830	3.865	3.855	3.840
125	3.740	3.755	3.760	3.760	3.770	3.775	3.780	3.780	3.780	3.770	3.825	3.810	3.795
150	3.685	3.800	3.800	3.795	3.785	3.775	3.765	3.755	3.735	3.715	3.770	3.755	3.735

Period T (s)	Group velocity (km/s)						
	W-82.0 N24.0	W-84.0 N24.0	W-82.0 N26.0	W-84.0 N26.0	W-76.0 N8.0	W-80.0 N8.0	W-82.0 N8.0
10	2.560	2.555	2.685	2.700	2.250	2.345	2.315
15	2.670	2.705	2.675	2.750	2.505	2.635	2.655
20	2.905	2.920	2.915	2.940	2.805	3.160	3.130
25	3.115	3.130	3.120	3.035	2.950	3.435	3.460
30	3.430	3.405	3.410	3.335	3.105	3.600	3.695
35	3.625	3.595	3.625	3.590	3.255	3.685	3.755
40	3.675	3.655	3.695	3.655	3.395	3.710	3.740
60	3.890	3.890	3.895	3.890	3.785	3.790	3.790
80	3.885	3.890	3.895	3.890	3.815	3.800	3.790
100	3.870	3.865	3.880	3.875	3.825	3.795	3.785
125	3.850	3.845	3.870	3.860	3.795	3.735	3.720
150	3.770	3.760	3.770	3.760	3.760	3.715	3.705

Appendix 2

See Table 3.

Table 3

Range of variability of the chosen velocity model (in Figs. 8, 9, 10) according with the parameterized layer thickness (h) and shear-wave velocity (V_s)

W-62N10		W-64N10		W-66N10		W-68N10		W-70N10	
h (km)	V_s (km/s)	*h* (km)	V_s (km/s)	*h* (km)	V_s (km/s)	*h* (km)	V_s (km/s)	*h* (km)	V_s (km/s)
0.3	0.00	0.1	0.00	0.2	0.00	0.1	1.20	0.5	1.10
0.5	1.20	0.5	1.20	0.1	1.23	0.6	2.10	0.5	2.10
3.2	2.20	2.0	2.20	1.0	1.98	2.0	3.88	6.0	3.40
2.7	2.20	2.0	2.20	1.9	1.98	2.0	3.88	6.0	3.40
18.0–22.0	3.53–3.63	3.5–5.5	2.56–2.76	2.0–4.0	2.93–3.13	20.0–24.0	3.25–3.40	7.5–12.5	3.10–3.30
10.5–15.5	3.97–4.17	17.0–27.0	3.59–3.79	21.5–26.5	3.55–3.75	6.0–11.0	3.88–4.05	7.0–10.0	3.38–3.62
29.0–34.0	4.45–4.55	25.0–30.0	4.40–4.60	20.0–40.0	4.40–4.60	42.0–52.0	4.40–4.60	40.0–50.0	4.38–4.62
30.0–70.0	4.65–4.75	30.0–70.0	4.65–4.75	20.0–42.5	4.65–4.70	20.0–40.0	4.60–4.70	30.0–55.0	4.60–4.80
55.0–105.0	4.40–4.60	105–130	4.40–4.60	110–140	4.40–4.60	90.0–110.0	4.40–4.60	80.0–110.0	4.40–4.60
W-72N10		W-74N10		W-76N10		W-78N10		W-80N10	
h (km)	V_s (km/s)	*h* (km)	V_s (km/s)	*h* (km)	V_s (km/s)	*h* (km)	V_s (km/s)	*h* (km)	V_s (km/s)
1.0	1.20	0.9	1.09	1.0	0.00	0.5	0.00	1.8	0.00
4.0	2.20	1.5	2.18	0.5	1.00	0.1	1.90	1.4	0.90
5.0	3.50	2.0	3.50	1.3	2.00	0.1	1.93	1.2	1.80
6.0	3.50	2.0	3.50	1.3	2.10	0.1	2.00	1.6	1.80
6.0–10.0	3.50–3.70	4.0–5.5	2.50–2.70	5.6–7.6	3.15–3.25	14.0–16.0	2.95–3.05	11.0–15.0	3.70–3.90
5.0–7.5	3.20–3.35	13.8–21.2	3.70–3.90	8.0–12.0	3.40–3.50	4.5–6.0	3.95–4.25	5.0–8.8	3.80–4.00
40.0–50.0	4.40–4.60	32.5–47.5	4.20–4.40	40.0–50.0	4.20–4.40	7.5–12.5	4.60–4.70	20.0–40.0	4.60–4.80
30.0–50.0	4.62–4.75	40.0–60.0	4.60–4.70	10.0–20.0	4.60–4.70	27.5–42.5	4.20–4.40	25.0–37.5	4.20–4.40
100–120	4.40–4.60	100–140	4.40–4.60	130–160	4.40–4.60	140–160	4.40–4.60	140–160	4.40–4.60
W-82N10		W-84N10		W-60N12		W-62N12		W-64N12	
h (km)	V_s (km/s)	*h* (km)	V_s (km/s)	*h* (km)	V_s (km/s)	*h* (km)	V_s (km/s)	*h* (km)	V_s (km/s)
1.8	0.00	1.0	1.10	1.8	0.00	0.4	0.00	1.4	0.00
1.0	1.10	3.5	2.60	2.0	1.53	6.0	2.56	1.5	2.05
4.0	3.30	4.0	2.60	4.0	2.16	2.0	3.07	1.3	2.50
4.2	3.30	4.5	3.50	7.0	3.39	14.0	3.24	3.0	3.30
4.5–6.8	3.42–3.58	5.0–6.0	3.45–3.55	7.0–9.0	4.05–4.15	11.0–17.0	3.88–4.08	13.0–17.0	3.20–3.40
8.0–14.0	3.70–4.00	10.0–12.0	4.00–4.20	9.5–12.5	3.33–3.43	15.0–22.5	4.16–4.41	7.5–12.5	3.83–4.07
32.5–52.5	4.60–4.80	52.5–57.5	4.60–4.70	45.0–50.0	4.62–4.75	20.0–30.0	4.38–4.62	40.0–50.0	4.38–4.62
40.0–70.0	4.20–4.40	17.5–22.5	4.10–4.20	30.0–45.0	4.12–4.38	65.0–85.0	4.38–4.62	65.0–80.0	4.38–4.62
127.5–150	4.40–4.60	145–160	4.45–4.55	40.0–65.0	4.40–4.60	60.0–85.0	4.60–4.80	50.0–90.0	4.40–4.60
W-66N12		W-68N12		W-70N12		W-72N12		W-74N12	
h (km)	V_s (km/s)	*h* (km)	V_s (km/s)	*h* (km)	V_s (km/s)	*h* (km)	V_s (km/s)	*h* (km)	V_s (km/s)
1.6	0.00	0.5	0.00	2.0	0.00	1.0	0.00	1.8	0.00
1.5	1.10	1.5	1.10	1.0	1.20	1.5	1.00	0.8	1.10
0.5	1.60	0.5	1.60	4.0	2.20	4.0	1.90	1.3	2.53
7.0	3.40	10.0	3.40	4.0	3.40	7.0	3.40	1.3	2.53
12.5–17.5	3.50–3.70	8.0–12.0	3.40–3.60	7.5–12.5	3.25–3.55	8.0–14.0	3.90–4.00	4.0–7.0	3.00–3.20
5.0–12.5	4.25–4.45	4.0–9.0	3.70–3.90	20.0–25.0	4.15–4.30	7.0–15.0	3.95–4.10	8.8–16.2	3.35–3.65
40.0–50.0	4.38–4.62	35.0–50.0	4.38–4.62	20.0–35.0	4.62–4.75	20.0–35.0	4.38–4.62	20.0–40.0	4.40–4.60
45.0–70.0	4.38–4.62	45.0–70.0	4.38–4.62	30.0–50.0	4.62–4.75	60.0–80.0	4.38–4.62	55.0–80.0	4.40–4.60
50.0–80.0	4.40–4.60	50.0–80.0	4.40–4.60	75.0–125.0	4.40–4.60	75.0–100.0	4.40–4.60	70.0–130.0	4.40–4.60

Table 3

continued

W-76N12		W-78N12		W-80N12		W-82N12		W-84N12	
h (km)	V_s (km/s)	*h* (km)	V_s (km/s)	*h* (km)	V_s (km/s)	*h* (km)	V_s (km/s)	*h* (km)	V_s (km/s)
2.8	0.00	2.4	0.00	3.0	0.00	1.5	0.00	1.6	1.10
0.1	0.64	0.2	2.35	0.6	1.10	1.0	0.64	2.0	2.65
0.1	0.66	0.3	2.40	1.0	1.12	0.5	1.93	4.0	2.65
0.1	1.96	0.1	2.60	1.5	2.00	1.0	1.93	5.1	3.50
6.2–8.8	3.33–3.48	9.0–11.0	3.17–3.23	5.0–7.5	4.00–4.20	5.0–8.0	3.45–3.55	5.5–8.5	3.35–3.65
7.5–12.5	3.30–3.38	5.5–8.5	3.38–3.43	11.8–19.2	3.70–3.90	10.0–20.0	3.80–3.95	7.5–12.5	3.95–4.10
20.0–30.0	4.20–4.40	25.0–35.0	4.40–4.60	18.0–36.0	4.60–4.80	30.0–50.0	4.40–4.60	35.0–55.0	4.50–4.70
27.5–42.5	4.40–4.60	20.0–30.0	4.20–4.40	85.5–108.0	4.40–4.60	50.0–75.0	4.20–4.40	20.0–50.0	4.10–4.25
140–160	4.40–4.60	140–160	4.40–4.60	75.0–105.0	4.40–4.60	100–140	4.40–4.60	130–160	4.40–4.60
W-60N14		W-62N14		W-64N14		W-66N14		W-68N14	
h (km)	V_s (km/s)	*h* (km)	V_s (km/s)	*h* (km)	V_s (km/s)	*h* (km)	V_s (km/s)	*h* (km)	V_s (km/s)
2.0	0.00	0.5	0.00	2.2	0.00	3.7	0.00	4.2	0.00
2.0	2.05	3.0	2.60	1.5	1.20	0.5	1.20	1.5	1.20
4.0	2.50	8.0	3.26	2.0	1.60	0.5	1.60	1.5	1.60
9.5	3.36	8.0	3.26	5.0	3.40	2.7	2.50	1.7	2.50
22.0–26.0	3.88–4.03	8.0–11.0	4.00–4.20	5.0–7.5	3.28–3.53	5.0–10.0	3.28–3.53	4.0–8.0	3.65–3.95
25.0–45.0	4.58–4.72	5.0–15.0	4.12–4.38	5.0–15.0	3.48–3.83	7.5–12.5	3.55–3.85	8.0–14.0	4.05–4.35
15.0–30.0	4.35–4.65	20.0–32.5	4.12–4.38	40.0–60.0	4.38–4.62	20.0–30.0	4.38–4.62	30.0–50.0	4.38–4.62
30.0–45.0	4.12–4.38	67.5–90.0	4.38–4.62	40.0–65.0	4.38–4.62	75.0–90.0	4.38–4.62	30.0–45.0	4.38–4.62
50.0–80.0	4.40–4.60	50.0–80.0	4.40–4.60	85.0–120.0	4.38–4.62	60.0–100.0	4.40–4.60	100–120	4.40–4.60
W-70N14		W-72N14		W-74N14		W-76N14		W-78N14	
h (km)	V_s (km/s)	*h* (km)	V_s (km/s)	*h* (km)	V_s (km/s)	*h* (km)	V_s (km/s)	*h* (km)	V_s (km/s)
2.8	0.00	3.0	0.00	3.0	0.00	1.9	0.00	2.7	0.00
1.5	1.10	0.1	0.84	0.1	0.64	2.3	1.20	0.4	0.64
2.0	1.60	0.5	2.80	0.1	2.30	0.3	1.80	0.6	2.50
7.0	3.40	0.6	2.80	0.1	2.40	0.3	2.50	0.8	2.50
5.0–7.0	3.35–3.65	4.0–6.0	3.60–3.70	5.0–6.5	3.50–3.55	9.0–11.0	3.60–3.80	4.0–6.0	3.50–3.70
11.0–17.0	4.65–4.80	10.5–13.5	3.25–3.35	12.5–15.5	3.20–3.30	4.0–8.0	3.25–3.35	10.0–12.0	3.10–3.30
10.0–15.0	4.38–4.52	5.0–6.5	4.00–4.10	17.5–32.5	4.58–4.72	10.0–20.0	4.35–4.45	14.5–22.0	4.75–4.80
30.0–45.0	4.60–4.80	20.0–30.0	4.60–4.70	30.0–50.0	4.40–4.60	35.0–65.0	4.40–4.60	80.0–100.0	4.45–4.55
100–120	4.40–4.60	140–160	4.40–4.60	140–160	4.40–4.60	140–160	4.40–4.60	100–140	4.43–4.57
W-80N14		W-82N14		W-84N14		W-60N16		W-62N16	
h (km)	V_s (km/s)	*h* (km)	V_s (km/s)	*h* (km)	V_s (km/s)	*h* (km)	V_s (km/s)	*h* (km)	V_s (km/s)
2.0	0.00	0.6	0.00	1.5	1.20	4.0	0.00	2.0	0.00
1.3	0.64	0.4	0.64	2.0	1.60	1.0	1.50	1.6	1.50
1.0	2.61	0.6	0.64	1.0	3.40	1.8	2.20	2.0	2.26
1.4	2.61	0.6	1.93	1.5	3.40	1.4	2.50	10.0	3.65
4.2–6.8	4.03–4.17	3.0–5.0	3.15–3.35	14.0–22.0	3.95–4.05	3.0–4.0	3.65–3.95	6.0–8.0	3.55–3.85
11.5–14.5	3.55–3.65	7.5–12.5	3.70–3.90	7.0–11.5	3.75–4.05	30.0–34.0	3.95–4.15	10.0–17.5	4.10–4.30
17.5–32.5	4.58–4.72	10.0–12.5	3.60–3.70	40.0–50.0	4.40–4.60	20.0–40.0	4.60–4.80	40.0–60.0	4.40–4.60
37.5–45.0	4.43–4.57	62.5–77.5	4.40–4.60	27.5–52.5	4.20–4.40	35.0–65.0	4.20–4.40	40.0–60.0	4.40–4.60
100–140	4.20–4.40	130–160	4.40–4.60	100–160	4.40–4.60	50.0–80.0	4.20–4.40	60.0–90.0	4.12–4.38
W-64N16		W-66N16		W-68N16		W-70N16		W-72N16	
h (km)	V_s (km/s)	*h* (km)	V_s (km/s)	*h* (km)	V_s (km/s)	*h* (km)	V_s (km/s)	*h* (km)	V_s (km/s)
2.0	0.00	3.9	0.00	2.1	0.00	2.6	0.00	2.5	0.00
1.5	1.20	1.5	1.20	0.2	0.64	0.4	0.62	0.6	0.64

Table 3

continued

W-64N16		W-66N16		W-68N16		W-70N16		W-72N16	
h (km)	V_s (km/s)	*h* (km)	V_s (km/s)	*h* (km)	V_s (km/s)	*h* (km)	V_s (km/s)	*h* (km)	V_s (km/s)
0.5	1.60	0.5	1.60	0.1	2.50	0.3	0.64	0.5	1.70
5.0	3.40	1.7	2.50	0.1	2.50	0.3	1.90	0.5	1.70
5.0–9.0	3.10–3.30	7.5–12.5	3.53–3.78	11.0–19.0	3.00–3.20	14.0–16.0	3.45–3.55	6.0–8.0	3.65–3.75
5.0–8.8	3.95–4.10	5.0–15.0	4.25–4.40	8.0–16.0	3.80–4.20	5.0–7.0	3.02–3.17	8.0–12.0	3.30–3.35
40.0–60.0	4.38–4.62	20.0–40.0	4.38–4.62	17.5–42.5	4.60–4.70	19.0–25.0	4.65–4.70	3.0–4.0	3.80–4.00
40.0–65.0	4.38–4.62	40.0–65.0	4.38–4.62	55.0–70.0	4.40–4.60	40.0–50.0	4.55–4.65	25.0–30.0	4.55–4.65
50.0–80.0	4.20–4.40	85.0–120.0	4.40–4.60	70.0–130.0	4.40–4.60	70.0–130.0	4.20–4.40	140–160	4.40–4.60
W-74N16		W-76N16		W-78N16		W-80N16		W-82N16	
h (km)	V_s (km/s)	*h* (km)	V_s (km/s)	*h* (km)	V_s (km/s)	*h* (km)	V_s (km/s)	*h* (km)	V_s (km/s)
2.6	0.00	2.5	0.00	2.1	0.00	1.2	0.00	0.2	0.00
0.2	2.40	0.8	0.64	1.0	0.64	1.3	0.84	1.0	1.10
0.1	2.50	0.7	3.40	2.8	2.60	1.0	2.40	0.5	1.93
0.3	2.60	1.7	3.45	6.0	3.45	2.0	2.40	0.6	1.93
4.5–5.2	3.50–3.70	12.5–15.5	3.27–3.33	2.5–3.8	2.95–3.15	5.0–8.0	3.50–3.70	5.0–7.0	3.50–3.70
10.0–15.0	3.10–3.20	4.0–6.5	3.50–3.90	8.2–10.8	3.67–3.83	8.8–16.2	3.50–3.70	17.5–22.5	3.80–4.00
5.0–15.0	4.10–4.20	10.0–17.5	4.20–4.40	50.0–60.0	4.60–4.70	30.0–50.0	4.50–4.70	30.0–35.0	4.40–4.60
22.5–47.5	4.40–4.60	10.0–25.0	4.40–4.60	70.0–80.0	4.43–4.57	65.0–90.0	4.40–4.60	17.5–32.5	4.20–4.40
140–160	4.40–4.60	167.5–190	4.40–4.60	70.0–80.0	4.40–4.60	65.0–115.0	4.40–4.60	140–160	4.40–4.60
W-84N16		W-86N16		W-60N18		W-62N18		W-64N18	
h (km)	V_s (km/s)	*h* (km)	V_s (km/s)	*h* (km)	V_s (km/s)	*h* (km)	V_s (km/s)	*h* (km)	V_s (km/s)
0.7	0.00	0.7	0.00	4.0	0.00	3.2	0.00	1.0	0.00
0.5	0.72	1.1	0.64	1.0	1.10	0.7	1.19	0.6	0.64
0.8	1.93	4.4	3.25	0.5	1.60	0.7	1.19	0.6	0.64
1.0	1.93	5.5	3.27	0.5	1.60	0.5	1.71	0.4	1.93
6.0–10.0	3.65–3.85	3.5–5.5	3.80–4.00	2.0–6.5	3.70–4.00	10.0–18.0	3.48–3.83	3.5–6.5	3.40–3.60
7.5–12.5	3.80–4.10	10.0–20.0	4.00–4.20	27.5–32.0	3.97–4.22	10.0–15.0	4.15–4.45	15.5–20.5	3.45–3.55
17.5–32.5	4.35–4.45	30.0–50.0	4.40–4.60	27.5–40.0	4.38–4.62	5.0–15.0	4.00–4.12	5.0–15.0	4.40–4.60
32.5–47.5	4.25–4.35	30.0–50.0	4.20–4.40	40.0–80.0	4.12–4.38	45.0–75.0	4.38–4.62	32.5–57.5	4.20–4.40
190–200	4.45–4.55	127.5–150	4.40–4.60	30.0–52.5	4.20–4.40	57.5–102.5	4.20–4.40	130–160	4.40–4.60
W-66N18		W-68N18		W-70N18		W-72N18		W-74N18	
h (km)	V_s (km/s)	*h* (km)	V_s (km/s)	*h* (km)	V_s (km/s)	*h* (km)	V_s (km/s)	*h* (km)	V_s (km/s)
1.7	0.00	2.1	0.00	1.9	0.00	0.9	0.00	1.2	0.00
0.6	0.64	0.3	0.64	0.2	1.10	0.6	1.10	0.3	1.20
0.8	1.60	0.8	1.60	0.3	1.10	0.5	1.80	0.2	2.10
0.8	1.60	0.8	1.60	0.4	1.60	0.6	1.80	0.2	2.10
2.5–3.8	3.05–3.15	7.0–11.0	3.55–3.65	10.0–14.0	3.38–3.53	2.0–3.0	2.77–2.92	5.8–8.2	3.20–3.30
19.8–22.2	3.55–3.65	5.0–7.5	3.20–3.40	10.0–12.5	3.10–3.30	17.5–20.5	3.45–3.55	13.0–17.0	3.35–3.45
7.5–12.5	4.60–4.70	7.5–11.2	3.20–3.40	32.5–47.5	4.35–4.65	30.0–50.0	4.40–4.60	47.5–62.5	4.45–4.55
40.0–50.0	4.40–4.60	55.0–65.0	4.40–4.60	20.0–35.0	4.40–4.60	20.0–40.0	4.40–4.60	40.0–70.0	4.50–4.70
140–160	4.40–4.60	135–150	4.40–4.60	140–160	4.40–4.60	155–170	4.40–4.60	100–160	4.40–4.60
W-76N18		W-78N18		W-80N18		W-82N18		W-84N18	
h (km)	V_s (km/s)	*h* (km)	V_s (km/s)	*h* (km)	V_s (km/s)	*h* (km)	V_s (km/s)	*h* (km)	V_s (km/s)
1.9	0.00	1.1	0.00	2.5	0.00	3.0	0.00	2.8	0.00
0.1	1.00	0.2	0.90	0.3	0.64	0.2	0.64	0.1	0.58
0.1	1.10	2.0	2.71	0.3	2.54	0.2	2.50	0.2	0.58
0.1	2.40	2.3	2.73	0.5	2.54	0.4	2.50	0.3	2.50

Table 3

continued

W-76N18		W-78N18		W-80N18		W-82N18		W-84N18	
h (km)	V_s (km/s)	*h* (km)	V_s (km/s)	*h* (km)	V_s (km/s)	*h* (km)	V_s (km/s)	*h* (km)	V_s (km/s)
5.8–7.2	3.00–3.20	12.5–13.5	3.25–3.35	17.5–22.5	3.67–3.73	10.0–12.0	4.05–4.15	17.5–22.0	4.00–4.10
12.5–15.5	3.30–3.50	5.0–12.5	4.20–4.40	2.0–4.5	3.85–4.15	12.0–16.0	3.60–3.80	5.5–10.5	3.97–4.22
45.0–55.0	4.40–4.60	25.0–40.0	4.40–4.60	12.5–22.5	4.20–4.40	20.0–40.0	4.55–4.65	60.0–75.0	4.30–4.50
15.0–27.5	4.60–4.70	50.0–70.0	4.40–4.60	22.5–37.5	4.40–4.60	30.0–60.0	4.20–4.40	15.0–30.0	4.20–4.40
140–160	4.40–4.60	100–120	4.40–4.60	175–190	4.45–4.55	140–160	4.40–4.60	120–140	4.40–4.60
W-86N18		W-70N20		W-72N20		W-74N20		W-76N20	
h (km)	V_s (km/s)	*h* (km)	V_s (km/s)	*h* (km)	V_s (km/s)	*h* (km)	V_s (km/s)	*h* (km)	V_s (km/s)
2.8	0.00	1.4	0.00	1.7	0.00	2.2	0.00	1.8	0.00
0.4	0.64	0.8	0.58	0.5	0.84	0.8	1.00	0.2	1.10
0.7	2.50	1.0	2.55	1.2	1.93	1.1	2.15	0.2	1.10
0.9	2.50	1.8	2.55	1.2	2.10	1.2	2.15	0.5	2.60
3.0–4.0	3.62–3.75	5.5–8.5	3.36–3.56	22.0–24.0	3.57–3.62	15.0–21.0	3.72–3.78	14.5–15.5	3.22–3.28
24.0–32.0	4.10–4.15	14.0–18.0	3.45–3.65	37.5–40.0	4.35–4.45	4.0–8.0	3.25–3.45	26.0–28.0	4.22–4.28
30.0–45.0	4.40–4.60	55.0–65.0	4.45–4.55	10.0–15.0	4.35–4.45	47.5–62.5	4.35–4.45	37.0–43.0	4.72–4.78
37.5–55.0	4.20–4.40	30.0–40.0	4.65–4.75	35.0–55.0	4.65–4.75	35.0–65.0	4.65–4.75	72.5–80.0	4.45–4.55
100–140	4.40–4.60	145–160	4.43–4.57	130–160	4.40–4.60	135–150	4.40–4.60	80.0–100	4.50–4.60
W-78N20		W-80N20		W-82N20		W-84N20		W-86N20	
h (km)	V_s (km/s)	*h* (km)	V_s (km/s)	*h* (km)	V_s (km/s)	*h* (km)	V_s (km/s)	*h* (km)	V_s (km/s)
2.8	0.00	2.5	0.00	2.9	0.00	2.7	0.00	2.8	0.00
0.3	1.20	0.7	1.10	0.1	0.81	0.5	0.90	0.1	1.10
0.4	1.22	0.5	2.60	0.2	0.81	0.7	2.25	0.1	2.50
0.6	2.50	0.8	2.60	0.4	3.40	1.0	2.50	0.2	2.80
3.0–4.0	3.72–3.88	16.5–19.5	3.65–3.75	22.0–26.0	3.67–3.77	10.0–14.0	4.00–4.20	18.0–26.0	3.60–3.80
13.0–19.0	3.35–3.65	17.5–20.0	4.28–4.53	23.8–30.0	4.30–4.50	6.0–8.5	3.25–3.55	8.0–11.5	4.05–4.35
10.0–15.0	4.53–4.67	30.0–50.0	4.30–4.50	20.0–30.0	4.20–4.40	15.0–30.0	4.35–4.45	35.0–50.0	4.30–4.50
22.5–37.5	4.33–4.47	25.0–35.0	4.60–4.80	30.0–50.0	4.40–4.60	85.0–100.0	4.40–4.60	40.0–60.0	4.35–4.65
190–200	4.50–4.60	130–160	4.40–4.60	127.5–150	4.40–4.60	100–120	4.40–4.60	100–140	4.40–4.60
W-82N22		W-84N22		W-86N22		W-82N24		W-84N24	
h (km)	*V*s (km/s)	*h* (km)	V_s (km/s)	*h* (km)	V_s (km/s)	*h* (km)	V_s (km/s)	*h* (km)	V_s (km/s)
0.8	0.00	1.7	0.00	1.1	0.00	0.7	0.00	2.2	0.00
0.1	1.10	0.7	1.10	0.4	0.64	2.3	1.93	0.4	1.30
0.2	2.30	2.0	2.40	1.0	2.20	1.0	2.40	0.5	1.70
0.3	2.30	2.3	2.40	1.6	2.20	1.2	2.40	0.5	1.70
13.0–15.0	3.15–3.25	12.5–17.5	3.60–3.80	4.5–10.5	3.25–3.45	14.0–18.0	3.55–3.65	17.5–22.5	3.55–3.65
17.0–19.0	3.85–3.95	5.0–7.5	3.95–4.25	15.0–25.0	3.75–3.95	10.0–22.0	4.10–4.30	10.0–20.0	4.15–4.30
7.5–12.5	4.65–4.75	35.0–50.0	4.40–4.60	25.0–45.0	4.35–4.65	22.5–37.5	4.40–4.60	15.0–22.5	4.05–4.35
17.5–32.5	4.25–4.35	50.0–70.0	4.40–4.60	20.0–40.0	4.40–4.60	25.0–40.0	4.60–4.70	32.5–57.5	4.60–4.70
140–160	4.45–4.55	70.0–130	4.40–4.60	130–160	4.40–4.60	140–160	4.40–4.60	130–160	4.40–4.60
W-82N26		W-84N26		W-76N8		W-80N8		W-82N8	
h (km)	V_s (km/s)	*h* (km)	V_s (km/s)	*h* (km)	V_s (km/s)	*h* (km)	V_s (km/s)	*h* (km)	V_s (km/s)
0.1	0.00	0.3	0.00	0.5	1.20	0.1	0.00	0.4	0.00
0.5	1.70	1.6	1.20	0.4	2.20	0.3	1.00	0.1	0.70
1.3	2.50	0.6	2.50	1.3	2.23	3.0	3.00	2.0	2.60
1.4	2.55	0.9	2.55	1.4	2.26	3.0	3.10	3.8	2.60
16.2–18.8	3.35–3.45	19.0–21.0	3.65–3.75	11.2–13.8	3.10–3.20	8.5–11.5	3.05–3.15	8.5–11.5	3.20–3.30
5.0–8.8	3.90–4.10	6.5–10.5	3.90–4.10	20.0–26.0	4.03–4.28	5.0–7.5	4.18–4.40	7.5–12.5	4.05–4.35

Table 3

continued

W-82N26		W-84N26		W-76N8		W-80N8		W-82N8	
h (km)	V_s (km/s)	h (km)	V_s (km/s)	h (km)	V_s (km/s)	h (km)	V_s (km/s)	h (km)	V_s (km/s)
17.5–32.5	4.20–4.40	15.0–25.0	4.18–4.32	25.0–35.0	4.20–4.40	40.0–50.0	4.40–4.60	30.0–50.0	4.60–4.70
30.0–60.0	4.60–4.70	42.5–50.0	4.65–4.70	20.0–30.0	4.60–4.70	10.0–25.0	4.10–4.20	22.5–47.5	4.20–4.40
140–160	4.40–4.60	140–160	4.40–4.60	140–160	4.40–4.60	130–160	4.40–4.60	110–140	4.40–4.60

The first four layer are fixed from a priori information. Frequently the chosen value does not necessarily fall in the center of the variability range that can turn out to be smaller than the step ΔP_i, used in the inversion

References

Álvarez, L. (1977), Dispersión de la velocidad de grupo de las ondas de Rayleigh en la región del Caribe. Informe Científico-Técnico No. 5, Instituto de Geofísica y Astronomía, La Habana, Cuba.

Bassin, C., Laske, G. and Masters, G. (2000), *The Current Limits of Resolution for Surface Wave Tomography in North America*, EOS Trans. AGU, *81*, F897.

Biswas, N.N. and Knopoff, L. (1974), *The structure of the upper mantle under the U.S. from the dispersión of Rayleigh waves, Geophys*. J. R. Astr. Soc. *36*, 515–539.

Boyadzhiev, G., Brandmayr, E., Pinat, T. and Panza, G.F., (2008) *Optimization for nonlinear inverse problem*. Rendiconti Lincei: Scienze Fisiche e Naturali, *19*, 17-43.

Chimera, G., Aoudia, A., Saraò, A. and Panza, G.F. (2003). *Active tectonics in central Italy: constraint from surface wave tomography and source moment tensor inversion*, Physics of the Earth and Planetary Interior. v. *138*, pp. 241–262.

Chulick, G. S. and Mooney, W. D. (2002), *Seismic Structure of the Crust and Uppermost Mantle of North America and Adjacent Oceanic Basins: A Synthesis*, Bull. Seism. Soc. Am., *92*(6), 2478-2492.

Dengo, G. and Case, J.E. (1990). "The Geology of North America. Volume H. The Caribbean Region", The Geological Society of America, Boulder, U.S.A.

Ditmar, P.G. and Yanovskaya, T.B. (1987), *A generalization of the Backus-Gilbert method for estimation of lateral variations of surface wave velocity*, Izv. Akad. Nauk SSSR, Fizika Zemli (6), 30–60.

Doglioni C., Gueguen E., Harabaglia P. and Mongelli F. (1999): *On the origin of W-directed subduction zones and applications to the western Mediterranean*. Geol. Soc. Sp. Publ., *156*, 541-561.

Doglioni C., Carminati E., Cuffaro M. and Scrocca D. (2007): *Subduction kinematics and dynamic constraints*. Earth Science Reviews, *83*, 125-175, doi:10.1016/j.earscirev.2007.04.001.

Doglioni C., Tonarini S. and Innocenti F., (2009), *Mantle wedge asymmetries and geochemical signatures along W- and E-NE-directed subduction zones*. Lithos, doi:10.1016/j.lithos.2009.01.012

Du, Z.J., Michelini, A., and Panza, G.F. (1998). *"EurID: a regionalised 3-D seismological model of Europe"*. Phys. Earth Planet. Inter., *105*, 31-62.

Fowler, C.M.R., The Solid Earth. An Introduction to Global Geophysics (Cambridge Univ. Press 1995).

González, O.; Alvarez, L.; Guidarelli, M.; Panza, G.F. (2007): *Crust and Upper Mantle Structure in the Caribbean Region by Group Velocity Tomography and Regionalization*. Pure and Applied Geophysics, v. *164*, pp. 1985–2007.

Grant, F.S. and West G.F., Interpretation Theory in Applied Geophysics (McGraw-Hill Inc., New York, U.S.A, 1965).

Growdon, M. A., Pavlis, G.L. Niu, F., Vernon, F.L. and Rendon, H. (2009) *Constraints on the mantle flow at the Caribbean-South American plate boundary inferred from shear wave splitting*, J. Geophys. Res. *114*, B02303, doi:10.1029/2008JB005887.

Iturralde, M. and Lidiak, E. (2000). Annual Reports of the project IGCP 433 "Caribbean Plate Tectonics, Origin and Evolution of the Region" (http://www.ig.utexas.edu/CaribPlate/CaribPlate.html)

Laske, G. and Masters, G. (1997), *A global digital map of sediment thickness*, EOS Trans. AGU *78*, F483.

Levshin, A.L., Pisarenko, V.F., and Pogrebinsky, G.A. (1972), *On a frequency-time analysis of oscillations*, Ann. Geophys. *28*(2), 211–218.

Levshin, A.L., Radnikova, L.I., and Berger, J. (1992), *Peculiarities of surface wave propagation across Central Eurasia*, Bull. Seismol. Soc. Am. *82*, 2464–2493.

Ligorría J.P. and Molina, E. (1997), *"Crustal Velocity Structure of Southern Guatemala using Refracted and Sp Converted Waves"*, Geofísica Intern., *36*(1).

Magnani, M.B., Zelt, C.A., Levander, A. and Schmitz, M. (2009), Crustal structure of the South-American plate boundary at 67° from controlled seismic data, J. Geophys. Res. *114*, B02312, doi: 10.1029/2008JB005817.

Mann, P., Prentice, C.S. Burr, G. Pena, L.R., Taylor, F.W. (1998): Tectonic evolution geomorphology and paleoseismology of the Septentrional fault system, Dominican Republic, In: Active strike-slip and Collisional Tectonics of the Northern Caribbean Plate Boundary Zone. Geological Society of America Special Paper 326, Geological Society of America, Boulder, Colorado, pp. 63-123.

Mann, P., Calais E., Ruegg J.-C., DeMets C., Jansma P. E., and Mattioli G. S. (2002): *Oblique collision in the northeastern Caribbean from GPS measurements and geological observations, Tectonics*, *21*(6), 1057, doi:10.1029/2001TC00134.

Miller, M.S., Levander, A., Niu, F. and Li, A. (2009), *Upper mantle structure beneath the Caribbean-South American plate boundary from surface wave tomography*, J. Geophys. Res. *114*, B01312. doi:10.1029/2007JB005507.

Montagner, J.P. and Kennett, B.L.N. (1996), *How to reconcile body-wave and normal-mode referente Earth models*, Geophys. J. Int. *125*, 229–248.

Mooney, W.D., Laske, G., and Masters, T.G. (1998), *CRUST 5.1: A global crustal model at 5° × 5°*, J. Geophys. Res. *103*(B1), 727–747.

Moreno, B., Grandison, M., and Atakan, K. (2002), *Crustal velocity model along the Southern Cuban margin: Implications for the tectonic regime at an active plate boundary,* Geophys. J. Int. *151*, 632–645.

Moreno, B. (2003), *The crustal structure of Cuba derived from Receiver Function Analysis*, Journal of Seismology, *7*, 359-375.

Panza, G.F., The Resolving power of seismic surface waves with respect to crust and upper mantle structural models, In The Solution of the Inverse Problem in Geophysical Interpretation (Cassinis, R. ed.) pp. 39–77.(Plenum Publ. Corp. 1981)

Panza, G.F., Doglioni C. and Levshin A. (2010): *Asymmetric ocean basins*. Geology, *38*, 1, p. 59-62, doi:10.1130/G30570.1.

Papazachos, B.C. (1964), *Dispersion of Rayleigh waves in the Gulf of Mexico and Caribbean Sea*, Bull. Seismol. Soc. Am. *54*(3), 909–926.

Pindell, J. and Kennan, L. (2001). "Kinematic Evolution of the Gulf of Mexico and Caribbean". In: GCSSEPM Research Conference (Richard Fillon, ed.), Houston, U.S.A.

Pindell, J. and Kennan, L. (2009). Tectonic evolution of the Gulf of Mexico, Caribbean and northern Sotuh America in the mantle reference frame: an update. In press in: The geology and evolution of the region between North and South America, Geological Society of London, Special Publication.

Pontevivo, A. and Panza, G. (2006). *The lithosphere–asthenosphere system in the Calabrian Arc and surrounding seas—southern Italy*. Pure and Applied Geophysics, v. *163*, pp. 1617–1659.

Santo, T. (1967), *Lateral variation of rayleigh waves dispersion character. Part IV: The Gulf of Mexico and Caribbean Sea*, Bull. Earthq. Res. Inst. *45*(4), 963.

Shapiro, N.M. y Ritzwoller, M.H. (2002). *Monte-Carlo inversion for a global shear velocity model of the crust and upper mantle*. Geophysics Journal International. *151*:88105.

Smith, W.H.F. and Sandwell, D.T. (1997). *Global sea floor topography from satellite altimetry and ship depth soundings*, Sci Magaz *277*, issue 5334.

Tarr, A.C. (1969), *Rayleigh waves dispersion in the North Atlantic Ocean, Caribbean Sea and the Gulf of Mexico*, J. Geophys. Res. *74*(6), 1591.

Ten Brink, Uri S., Coleman, Dwight F., and Dillon, William P. (2001). Asymmetric seafloor spreading, crustal thickness variations and transitional crust in Cayman trough from gravity, Paper No. 63-0 GSA Annual Meeting, November 5-8, 2001. Boston, Massachusetts.

Ten Brink, U.S., Coleman, D.F., and Dillon, W.P. (2002). *The nature of the crust under Cayman Trough from gravity*. Marine and Petroleum Geology, v. *19*, pp. 971-987.

Tenreyro, R., López, J. G., Echevarría, G., Alvarez, J., Sánchez, J. R. (1994). Geologic Evolution and Structural Geology of Cuba. Abstracts AAPG Annual Meeting, June 12- 15. Denver. Colorado.

Urban, L., Cichowicz, A. and Vaccari, F. (1993). *"Computation of Analytical Partial Derivatives of Phase and Group Velocities of Rayleigh Waves Respect to Structural Parameters"*. Studia Geoph. Et Geod., *36*, 14-36.

Valyus, V.P. (1968), Determining seismic profiles from a set of observations (in Russian), Vychislitielnaya Seismologiya 4, 3–14. English translation: Computational Seismology (V.I. Keylis-Borok, ed.) pp. 114–118, (Consultants Bureau, 1972).

Van der Hilst, R. D. (1990): "Tomography with P, PP and pP Delay-time Data and the Three-dimensional Mantle Structure below the Caribbean Region", Ph.D. Thesis, University of Utrecht, Holland.

Vdovin, O., Rial, J.A., Levshin, A.L. and Ritzwoller, M. H. (1999). *"Group-velocity Tomography of South America and the Surrounding Oceans"*. Geophys. J. Int., *136*, 324-340.

Wu, F.T. and Levshin, A. (1994), *Surface-wave group velocity tomography of east Asia*, Phys. Earth Planet Int. *84*, 59–77.

Yanovskaya, T.B. and Ditmar, P.G. (1990), *Smoothness criteria in surface wave tomography*, Geophys. J. Int. *102*, 63–72.

Yanovskaya, T.B. (1997), *Resolution estimation in the problems of seismic ray tomography*, Izvestiya, Physics of the Solid Earth *33*(9), 762–765.

(Received June 30, 2010, revised March 9, 2011, accepted March 14, 2011, Published online June 1, 2011)